Same-sign Charged Higgs Pair Production in bosonic decay channels at the HL-LHC and HE-LHC

Abdesslam Arhrib[1,2], Kingman Cheung[2,3,4], Chih-Ting Lu[5]

[1] *Département de Mathématique, Faculté des Sciences et Techniques, Université Abdelmalek Essaadi, B. 416, Tangier, Morocco*

[2] *Physics Division, National Center for Theoretical Sciences, Hsinchu, Taiwan 300*

[3] *Department of Physics, National Tsing Hua University, Hsinchu 300, Taiwan*

[4] *Division of Quantum Phases and Devices, School of Physics, Konkuk University, Seoul 143-701, Republic of Korea*

[5] *School of Physics, KIAS, Seoul 130-722, Republic of Korea*

(Dated: November 18, 2020)

Abstract

Same-sign charged Higgs pair production via vector-boson scattering is a useful probe of the mass spectrum among the heavier scalar, pseudoscalar, and charged Higgs bosons in two-Higgs-doublet models. It has been shown that the production cross section scales as the square of the mass difference $\Delta m = (m_{H^0} - m_{A^0})$ in the alignment limit ($\cos(\beta - \alpha) = 0$). We study the potential measurement of this same-sign charged Higgs pair production at the high-luminosity LHC (HL-LHC) and the proposed 27 TeV pp collider, with emphasis in the decay channel $H^\pm H^\pm \to (W^\pm A^0)(W^\pm A^0)$, which is in general the dominant mode when the charged Higgs mass is above the $W^\pm A^0$ threshold. We also examine the current allowed parameter space taking into account the theoretical constraints on the model, the electroweak precision test (EWPT) measurements, B decays, and direct searches in the $H^\pm \to \tau^\pm \nu_\tau$ and $H^\pm \to W^\pm A^0 \to (\ell^\pm \nu_\ell)(\mu\mu)$.

I. INTRODUCTION

Since the discovery of a Higgs-like particle at the CERN Large Hadron Collider (LHC) in 2012, there have been many theoretical and phenomenological studies dedicated to non-minimal Higgs sector models that can explain the observed Higgs-like particle and account for some weakness of the Standard Model (SM). One common feature of many extensions of the minimal Higgs sector is the presence of extra neutral Higgs bosons as well as singly-charged Higgs bosons in the physical spectrum. Therefore, the discovery of charged Higgs bosons would be an unambiguous sign of physics beyond the SM. One of the most popular models with extended Higgs sector is the two-Higgs-Doublet Model (2HDM) [1, 2] in which one introduces two Higgs doublet fields to break the $SU_L(2) \times U_Y(1)$ symmetry down to the $U(1)_{\rm em}$ symmetry. In order to avoid tree-level flavor-changing neutral current couplings, one can advocate a natural flavor conservation imposed by a discrete Z_2 symmetry [3]. Depending on the Higgs and fermion field transformations under the Z_2, one can have a number of Yukawa textures for the fermion sector, denoted by Type I, II, X, and Y 2HDM's. After electroweak symmetry breaking driven by the two Higgs fields takes place, the physical spectrum of the model consists of 2 CP-even Higgs bosons h^0, H^0 (one of them could be identified as the observed 125 GeV Higgs-like particle), a CP-odd Higgs boson A^0 and a pair of charged Higgs bosons $H^\pm$.

At hadron colliders, charged Higgs bosons can be produced in a number of channels. An important source of light charged Higgs bosons is from $t\bar{t}$ production, followed by the top decay into a charged Higgs boson and a bottom quark if kinematically allowed. Other important mechanisms for singly-charged Higgs production are the QCD processes $gb \to tH^-$ and $gg \to t\bar{b}H^-$ [4]. We refer to Ref. [5] for an extensive review on charged Higgs phenomenology. Charged Higgs bosons have been searched for in the past at both LEP [6] and Tevatron [7]. An upper limit of the order of 80 GeV has been set at LEP experiments both from fermionic and bosonic decays $H^\pm \to W^\pm A^0$ [6]. While at the Tevatron a search for the charged Higgs from top decay had been performed in various decay channels of $H^\pm$ and limits on $B(t \to H^+ b)$ have been set [7]. At the LHC, one can search for light $H^\pm$ from top decay and for heavy $H^\pm$ from $gb \to tH^-$ and $gg \to t\bar{b}H^-$. Light charged Higgs boson ($\leq m_t - m_b$) would decay dominantly into $\tau\nu_\tau$, $c\bar{s}$ or $c\bar{b}$ final states. In case of light pseudoscalar boson A^0, $H^\pm$ can also decay into $W^\pm A^0$. However, a heavy H^+ can also decay

into $t\bar{b}$, W^+h^0, W^+A^0, or W^+H^0 if kinematically open. Both at the LHC Run-1 and Run-2, ATLAS and CMS had already set exclusion limits on $B(t \to bH^+) \times B(H^+ \to \tau^+\nu_\tau)$ [8–13], which can be used to set limits on $\tan\beta$ for a given charged Higgs mass less than $\leq m_t - m_b$. Moreover, from $t \to bH^+$ there has been also a search for $H^+ \to c\bar{s}$ channel both by ATLAS and CMS [14] at 7 TeV and 8 TeV. The limit obtained on $B(t \to bH^+)$ is rather weak compared to the $\tau\nu_\tau$ mode. Both ATLAS and CMS also searched for $H^\pm \to tb$ decay, in which no $H^\pm$ signal was observed and upper limits on the $\sigma(pp \to tbH^\pm) \times B(H^\pm \to tb)$ are set [15–18].

In the 2HDM, it has been shown [19–21] that the charged Higgs boson can decay dominantly into the bosonic final state $H^\pm \to W^\pm A^0$ when kinematically open. Other models beyond SM could also have similar features such as 2HDM with singlet scalars [22] and also the next-to-minimal supersymmetric standard model [23]. At LEPII [24], pair-produced charged Higgs bosons have been searched in various final states, including $\tau^+\nu_\tau\tau^-\bar{\nu}_\tau$, $c\bar{s}\bar{c}s$, $c\bar{s}\tau^-\bar{\nu}_\tau$, W^*AW^*A and $W^*A\tau^-\bar{\nu}_\tau$, and an upper limit of the order 80 GeV was set on the charged Higgs mass. Recently, CMS also performed a search for such bosonic decays of the charged Higgs [25]. The study was only dedicated to light charged Higgs produced from top decay followed by $H^\pm \to W^\pm A^0$, where A^0 decays into a pair of muons and $W^\pm$ decays into a charged lepton (e, μ) and a neutrino. Assuming that $H^\pm$ decays 100% into $W^\pm A^0$ and $B(A^0 \to \mu\mu) = 3 \times 10^{-4}$, CMS set a new and first limit from bosonic decay of $H^\pm$ on $B(t \to bH^+)$.

Recently, Ref. [26] proposed a new mechanism where a pair of same-sign charged Higgs bosons are produced via vector boson fusion (VBF) at hadron colliders. Such a process can shade some light on the global symmetry of the underlying scalar potential. Assuming that the charged Higgs bosons decay into $\tau\nu_\tau$ or tb, Ref.[26] evaluated the signal and the SM backgrounds, and discussed the feasibility of the new process both for the high-luminosity LHC (HL-LHC) with 14 TeV center of mass energy and also for the future high-energy LHC (HE-LHC) 27 TeV.

In this work, motivated by the recent CMS search for the bosonic decay $H^\pm \to W^\pm A^0$, we investigate same-sign charged Higgs production from VBF, followed by bosonic decays of the charged Higgs boson:

$$pp \to jjW^{\pm *}W^{\pm *} \to jjH^\pm H^\pm \to jj(W^\pm A^0)(W^\pm A^0) \; . \tag{1}$$

in Type-I and X 2HDM's. We calculate the signal and various SM backgrounds, and estimate the sensitivity at the HL-LHC as well as for the future hadron collider HE-LHC with 27 TeV center of mass energy. Another important observation that motivates our work is because the fermionic production modes for these new scalars are highly suppressed by large $\tan\beta$ in both Type-I and Type-X 2HDMs, the discovery of these new scalars via fermionic modes is indeed challenging at the LHC. Therefore, we are exploring the bosonic decay mode of the charged scalar $H^\pm \to W^\pm A^0$, which dominates for $\tan\beta > 5$.

We should emphasize, instead of studying each new scalar (or two of them) in different processes separately, the novel process we consider here involves the effects of all new scalar masses. It means that we have the chance to simultaneously test the whole mass spectrum in the 2HDM for some specific mass relations via a single process. Finally, we show that the mass spectrum of $m_{A^0} = 63 - 100$ GeV and $\Delta m \equiv m_{H^0} - m_{A^0} = 200 - 250$ GeV in Type-I and X 2HDM's can be explored at the HE-LHC in the future after the accelerator and detector are further upgraded.

The strategy in this work is two-fold. If any new scalar has been discovered in the future, the signal process considered here serves to confirm or rule out some specific mass spectra in the 2HDMs. On the other hand, if we do not find any positive evidence of new scalars in the future, the signal process in this study can also help to clarify which kind of mass spectra in 2HDMs is not preferred.

The organization is as follows. In the next section, we describe briefly the 2HDM's and relevant interactions. In Sec. III, we discuss the constraints on the model from theoretical requirements, electroweak precision test measurements, B decays, and direct searches. In Sec. IV, we calculate the same-sign charged Higgs production cross sections, and perform the signal-background analysis. We conclude in Sec. V.

II. BRIEF REVIEW OF TWO-HIGGS-DOUBLET MODELS

Many beyond Standard Model process an extended Higgs sector with more Higgs doublets, Higgs singlets , Higgs triplets or a mixture of all. One of the simplest, popular and well motivated extension of the SM is the two Higgs doublets model. A variety of which can be used in the minimal supersymmetric SM. In the two-Higgs-Doublet Model (2HDM), two Higgs doublet fields $\Phi_{1,2}$ with hypercharge $Y_{\Phi_{1,2}} = 1/2$ are introduced. The most general

renormalizable scalar potential, which respects the $SU_L(2) \otimes U_Y(1)$ gauge symmetry, has the following form:

$$\begin{aligned} V(\Phi_1,\Phi_2) = & \, m_{11}^2\, \Phi_1^\dagger \Phi_1 + m_{22}^2\, \Phi_2^\dagger \Phi_2 + \left(m_{12}^2\, \Phi_1^\dagger \Phi_2 + h.c \right) + \frac{\lambda_1}{2} \left(\Phi_1^\dagger \Phi_1 \right)^2 + \frac{\lambda_2}{2} \left(\Phi_2^\dagger \Phi_2 \right)^2 \\ & + \lambda_3\, \Phi_1^\dagger \Phi_1\, \Phi_2^\dagger \Phi_2 + \lambda_4\, \Phi_1^\dagger \Phi_2\, \Phi_2^\dagger \Phi_1 + \left[\frac{\lambda_5}{2} \left(\Phi_1^\dagger \Phi_2 \right)^2 + h.c \right] \\ & + \left[\left(\lambda_6 \left(\Phi_1^\dagger \Phi_1 \right) + \lambda_7 \left(\Phi_2^\dagger \Phi_2 \right) \right) \left(\Phi_1^\dagger \Phi_2 \right) + h.c \right] \end{aligned} \tag{2}$$

where m_{11}^2, m_{22}^2 and $\lambda_{1,2,3,4}$ are real, while m_{12}^2 and $\lambda_{5,6,7}$ could be complex for CP violation purpose. If we require that the potential to be invariant under a discrete Z_2 symmetry $\Phi_1 \to \Phi_1$, $\Phi_2 \to -\Phi_2$ which is needed for natural flavor conservation in the Yukawa sector (see discussion below), this would lead to $\lambda_{6,7} = 0$. One can still allow a soft violation of the discrete symmetry by a dimension two terms m_{12}^2. In what follow, we assume that $\lambda_{6,7} = 0$ and $m_{12}^2 \neq 0$.

Assuming that both Φ_1 and Φ_2 acquire a vacuum expectation value (VEV) $v_{1,2}$ that can induce electroweak symmetry breaking, the two complex scalar $SU_L(2)$ doublets can be decomposed according to

$$\Phi_i = \begin{pmatrix} \phi_i^+ \\ \left(v_i + \rho_i + i\eta_i \right) / \sqrt{2} \end{pmatrix}, \quad i = 1, 2\,. \tag{3}$$

The mass eigenstates for the Higgs sector are obtained by orthogonal transformations,

$$\begin{pmatrix} \phi_1^\pm \\ \phi_2^\pm \end{pmatrix} = R_\beta \begin{pmatrix} G^\pm \\ H^\pm \end{pmatrix}, \quad \begin{pmatrix} \rho_1 \\ \rho_2 \end{pmatrix} = R_\alpha \begin{pmatrix} H^0 \\ h^0 \end{pmatrix}, \quad \begin{pmatrix} \eta_1 \\ \eta_2 \end{pmatrix} = R_\beta \begin{pmatrix} G^0 \\ A^0 \end{pmatrix}, \tag{4}$$

with the generic form ($\theta = \alpha, \beta$)

$$R_\theta = \begin{pmatrix} \cos\theta & -\sin\theta \\ \sin\theta & \cos\theta \end{pmatrix}.$$

From the eight degrees of freedom initially present in the two scalar doublets, three of them, namely the Goldstone bosons $G^\pm$ and G^0, are eaten by the longitudinal component of $W^\pm$ and Z^0, respectively. The remaining five degrees of freedom should manifest as physical Higgs bosons: two CP-even H^0 and h^0, one CP-odd A^0, and a pair of charged scalars $H^\pm$. In the CP conserving case, the above potential contains 10 parameters (including the VEV's of the Higgs doublets). m_{11}^2 and m_{22}^2 can be eliminated by the use of the 2 minimization

conditions. One of the VEV's can be traded from the W mass as a function of the ratio $\tan\beta \equiv v_2/v_1$. We are then left with seven independent parameters which can be taken as: the four physical masses m_h, m_H, m_A and $m_{H\pm}$, CP-even mixing angle α, $\tan\beta$ and m_{12}^2.

In the Yukawa sector, it is well known that if we assume that both Higgs doublets couple to all fermions we will end up with large Flavor-Changing Neutral Currents (FCNC) mediated by the neutral Higgs scalars at tree level. In order to avoid such FCNC's, a discrete Z_2 symmetry (where $\Phi_1 \to \Phi_1$ and $\Phi_2 \to -\Phi_2$) is imposed [3]. Note that in the above potential, the Z_2 symmetry is only violated by the dimension-two term involving m_{12}^2. Depending on the Z_2 charge assignment to the lepton and quark fields [2, 27, 28], one can have 4 different types of Yukawa textures. [1] In the type-I model, only the second doublet Φ_2 interacts with all the fermions like in the SM while in the type-II model Φ_1 interacts with the charged leptons and down-type quarks and Φ_2 interacts with up-type quarks. In the type-X (lepton-specific) model, charged leptons couple to Φ_1 while all the quarks couple to Φ_2. Finally, in the type-Y (flipped) model down-type quarks acquire masses from their couplings to Φ_1 while charged leptons and up-type quarks couple to Φ_2. The most general Yukawa interaction can be written as follows [2],

$$-\mathcal{L}_{\rm Yukawa}^{\rm 2HDM} = \overline{Q}_L Y_u \widetilde{\Phi}_2 u_R + \overline{Q}_L Y_d \Phi_d d_R + \overline{L}_L Y_\ell \Phi_\ell \ell_R + \text{h.c}, \tag{5}$$

where $\Phi_{d,l}$ $(d,l=1,2)$ represent Φ_1 or Φ_2, Y_f ($f = u, d$ or ℓ) stand for 3×3 Yukawa matrices and $\widetilde{\Phi}_2 = i\sigma_2 \Phi_2^\star$.

Writing the Yukawa interactions Eq. (5) in terms of the mass eigenstates of the neutral and charged Higgs bosons yields

$$\begin{aligned} -\mathcal{L}_{\rm Yukawa}^{\rm 2HDM} = & \sum_{f=u,d,\ell} \frac{m_f}{v}\left(\xi_f^{h^0}\overline{f}fh^0 + \xi_f^{H^0}\overline{f}fH^0 - i\xi_f^{A^0}\overline{f}\gamma_5 fA^0\right) \\ & + \left\{\frac{\sqrt{2}V_{ud}}{v}\,\overline{u}\left(m_u\xi_u^{A^0}\mathrm{P}_L + m_d\xi_d^{A^0}\mathrm{P}_R\right)dH^+ + \frac{\sqrt{2}m_\ell\xi_\ell^{A^0}}{v}\,\overline{\nu_L}\ell_R H^+ + \text{h.c}\right\}, \end{aligned} \tag{6}$$

where $v^2 = v_1^2 + v_2^2 = (2\sqrt{2}G_F)^{-1}$; P_R and P_L are the right- and left-handed projection operators, respectively. The coefficients for $\xi_f^{A^0}$ $(f = u, d, l)$ in the four 2HDM types, which are relevant to this work, are given in the Table I.

[1] Here we follow the same notation as in Ref. [27].

type	$\xi_u^{A^0}$	$\xi_d^{A^0}$	$\xi_l^{A^0}$
I	$\cot\beta$	$-\cot\beta$	$-\cot\beta$
II	$\cot\beta$	$\tan\beta$	$\tan\beta$
X	$\cot\beta$	$-\cot\beta$	$\tan\beta$
Y	$\cot\beta$	$\tan\beta$	$-\cot\beta$

TABLE I. Yukawa coupling coefficients $\xi_f^{A^0}$ to the up-quarks, down-quarks and the charged leptons ($f = u, d, l$) in the four 2HDM types.

III. CONSTRAINTS

We consider both theoretical and experimental constraints on 2HDM's.

A. Theoretical and electroweak precision constraints

For theoretical constraints we take into account all set of tree-level perturbative unitarity conditions [29–31]. We use the unitarity constraints from Ref.[31] and require that the eigenvalues of the scattering amplitudes satisfy the original Lee-Quigg-Thacker bound [29]. We also require that all λ_i's remain perturbative. Moreover, we demand that the potential remains bounded from below when the Higgs fields become large in any direction of the field space [2], which results in the following set of constraints:

$$\lambda_1 > 0 \ , \ \lambda_2 > 0 \ , \ \sqrt{\lambda_1\lambda_2} + \lambda_3 + \min(0, \lambda_4 + \lambda_5, \lambda_4 - \lambda_5) > 0 \ . \tag{7}$$

For experimental constraints we can further divide them into indirect and direct searches. The indirect searches mainly arise from Electro-Weak Precision Observables (EWPOs) and flavor physics. The EWPOs can be represented by a set of oblique parameters S, T and U. From 2018 Particles Data Group (PDG) review [32] with a fixed $U = 0$, the best fit of S, T parameters can be represented as $S = 0.02 \pm 0.07$ and $T = 0.06 \pm 0.06$. We emphasize that the T parameter, which is related to the amount of isospin violation, is sensitive to the mass splitting among $H^\pm$, H^0, and A^0. It will restrict the allowed mass spectrum for the scalars in our analysis below. In order to fulfill the T constraint in the 2HDM, the spectrum should be chosen close to the approximate custodial symmetry [33], which is satisfied in one

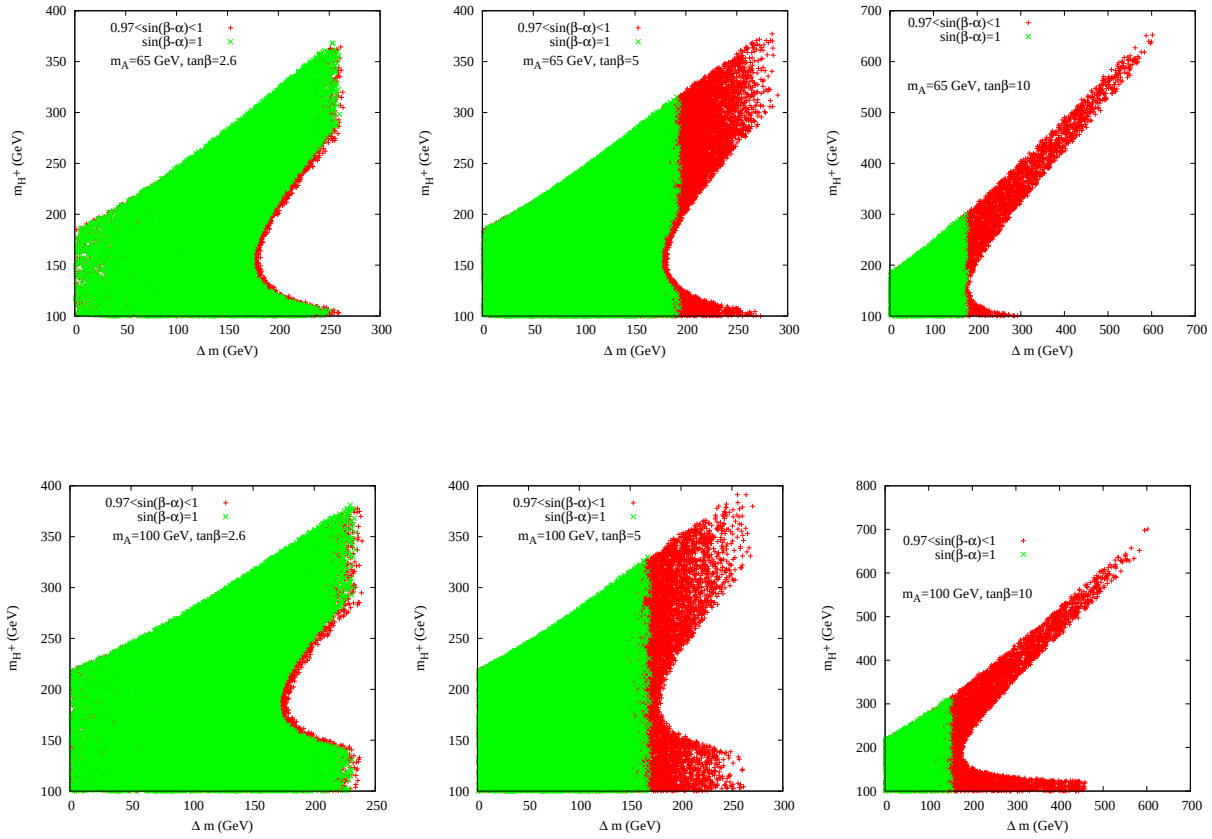

FIG. 1. The allowed parameter space in the plane of ($\Delta m \equiv m_{H^0} - m_{A^0}$, $m_{H^\pm}$) due to the constraints from the oblique S and T parameters, and all theoretical constraints. The upper panels are for $m_{A^0} = 65$ GeV while the lowers for $m_{A^0} = 100$ GeV, in which $\tan\beta = 2.6$ (left), 5 (middle), and 10 (right) are shown. The green points are right at the alignment limit $\sin(\beta-\alpha) = 1$ while the red points satisfy $0.97 < \sin(\beta-\alpha) < 1$ (near alignment limit).

of the following limits: i) $m_{H^\pm} = m_{A^0}$, ii) $m_{H^\pm} = m_{H^0}$ together with $\sin(\beta-\alpha) = 1$, or iii) $m_{H^\pm} = m_{H^0}$ together with $\cos(\beta-\alpha) = 1$.

As mentioned before, the oblique parameter T is highly sensitive to the mass splitting among $H^\pm$, H^0, and A^0. [2] In order to obtain the allowed parameter space for the mass of

[2] Here we assume the SM-like Higgs boson is the lightest CP-even scalar ($m_{H^0} > m_{h^0}$). For the reversed case $m_{H^0} = 125$ GeV and $m_{h^0} < m_{H^0}$, with another near alignment limit of $\cos(\beta-\alpha)$ one can also consider another process

$$pp \to jjW^{\pm *}W^{\pm *} \to jjH^\pm H^\pm \to jj(W^\pm h^0)(W^\pm h^0)\,,$$

which is similar to the process considered in this work.

charged Higgs boson and the mass splitting $\Delta m = m_{H^0} - m_{A^0}$, we consider all the above theoretical constraints and 3σ allowed regions of the S and T parameters in Fig. 1 for $\tan\beta = 2.6$, 5, and 10 with $m_{A^0} = 65$ and 100 GeV, respectively. We also scan on m_{12}^2 in the following range $[0, 10^6]$ GeV^2 in order to satisfy the perturbative unitarity and vacuum stability constraints for a fixed set of physical masses and mixings. We notice that, in our parameter space, the S parameter is always within the best-fit range while the T parameter severely constrains the splitting between m_{A^0} and $m_{H^\pm}$, and also Δm.

For $\tan\beta = 2.6$, there is no significant difference in the allowed region between the alignment limit $\sin(\beta-\alpha) = 1$ and the near-alignment limit $0.97 < \sin(\beta-\alpha) < 1$. In the case where $\tan\beta = 5$, one can see that Δm is constrained to be less than about 200 GeV in the exact alignment limit. This cut on Δm is in fact due to the vacuum stability constraints in Eq.(7), where either λ_1 or the third constraint in Eq.(7) becomes quickly negative. While in the case near-alignment limit $0.97 < \sin(\beta-\alpha) < 1$, which allows the vacuum stability to be fulfilled and Δm can reach up to 280 GeV. This correlation between vacuum stability and $\sin(\beta-\alpha) \in [0.97, 1]$ is also observed in the case $\tan\beta = 10$ and is even more pronounced where one can see that Δm can reach up to 600 GeV. The parameter space can be divided into two parts. The first region of parameter space is for light $H^\pm$. Once $m_{H^\pm} \sim m_{A^0}$, the mass splitting Δm can be as large as $300 - 450$ GeV. The second region is for heavy $H^\pm$. When $m_{H^\pm} \sim m_{H^0}$, the mass splitting Δm can be extended to about 600 GeV for $\tan\beta = 10$. While in the case $\tan\beta = 5$, the maximum mass splitting Δm is less than 200 GeV in the alignment limit $\sin(\beta-\alpha) = 1$, and could be extended to more than 250 GeV for $0.97 < \sin(\beta-\alpha) < 1$. We stress that even in the case where Δm is rather small, the T parameter severely constrains the charged Higgs mass to be less than about 200 GeV for $\tan\beta = 2.6, 5$ and 10.

B. B physics constraints

The most severe constraints in flavor physics are due to the measurements of $B(B \to X_s\gamma)$, $B(B_{d,s} \to \mu^+\mu^-)$ and Δm_s of B mesons. For $B(B \to X_s\gamma)$, according to the latest analysis by [34], we have:

- In 2HDM type-II and Y, the $b \to s\gamma$ constraint forces the charged Higgs mass to be heavier than 580 GeV [34, 35] for any value of $\tan\beta \geq 1$.

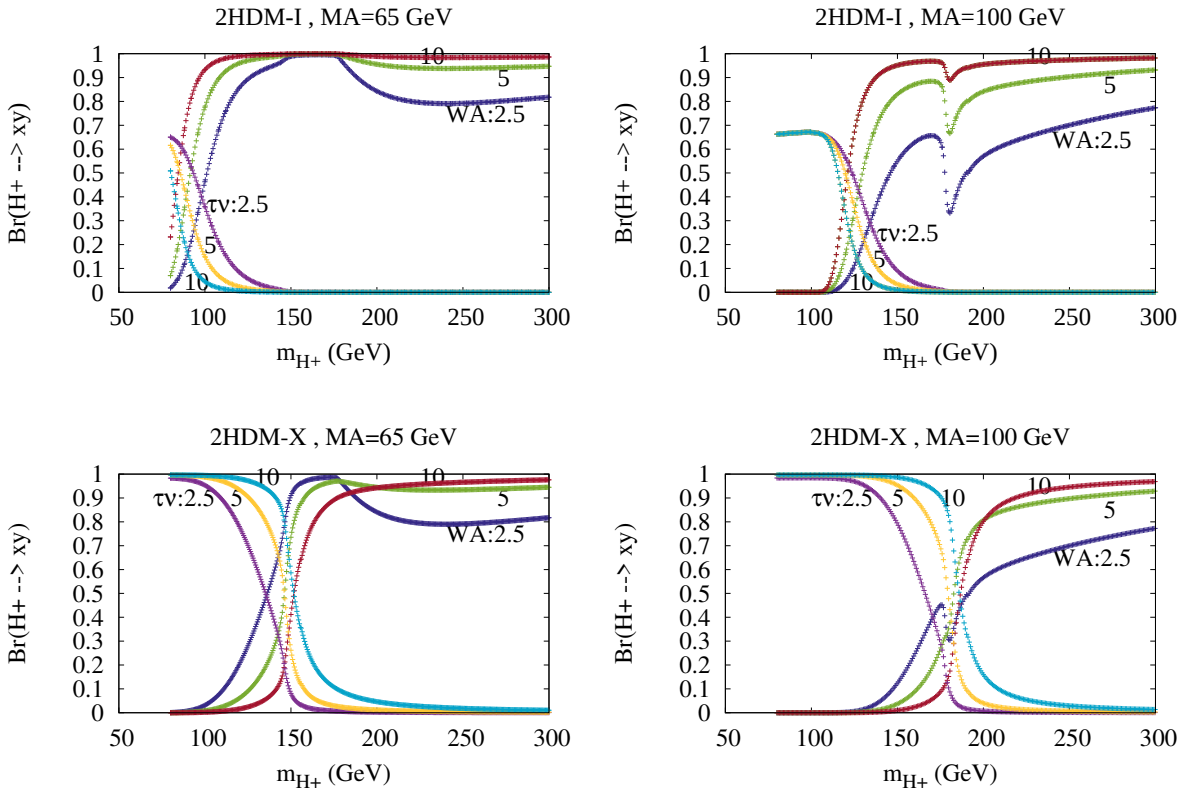

FIG. 2. Branching fractions of the charged Higgs boson versus $m_{H^\pm}$ for type-I 2HDM with $m_{A^0} = 65$ GeV (upper-left panel), $m_{A^0} = 100$ GeV (upper-right panel) and for type-X 2HDM with $m_{A^0} = 65$ GeV (lower-left panel), $m_{A^0} = 100$ GeV (lower-right panel). The alignment limit $\sin(\beta - \alpha) = 1$ is assumed.

- In 2HDM-I and X, charged Higgs with mass as low as $\sim 100 - 200$ GeV [34, 36] is still allowed as long as $\tan\beta \geq 2$.

For other B-physics observables we refer to the recent analysis [37], in which they also included Δm_s and $B_{d,s} \to \mu^+\mu^-$. For a light charged Higgs boson, $100 < m_{H^\pm} < 200$ GeV, of interest in this study, one can conclude from [37] that $\tan\beta \geq 3$ is allowed for 2HDM type I and X.

C. $H^\pm$ and A^0 branching ratios and Direct searches

Before discussing the constraints coming from direct searches, we first show the branching ratios of $H^\pm$ and A^0 in both 2HDM type I and X in the following subsection. Calculations

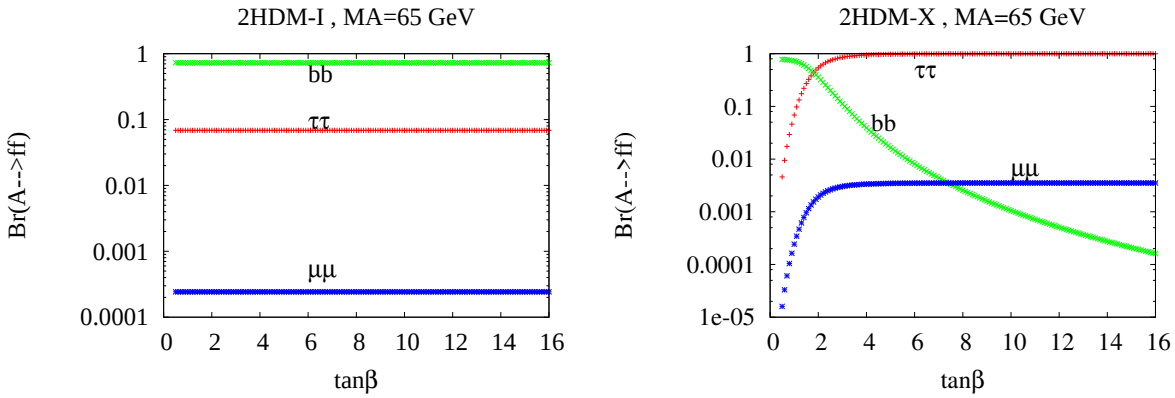

FIG. 3. Branching fractions of the CP-odd Higgs boson A^0 versus $\tan\beta$ for $m_{A^0} = 65$ GeV in type-I 2HDM (left panel) and type-X 2HDM (right panel).

of these branching ratios are performed using the public code **2HDMC** [38].

1. *Branching ratios of $H^\pm$ and A^0*

We illustrate in Fig. 2 the branching ratios of the charged Higgs boson for both 2HDM type I and X. It is clear that once the bosonic decay mode $H^\pm \to W^\pm A^0$ is open, it can be the dominant decay mode and both $B(H^+ \to t\bar{b})$ and $B(H^\pm \to \tau^\pm \nu_\tau)$ are highly suppressed.

In type I, one can see that the full dominance of the bosonic decay needs $\tan\beta > 5$ which reduces the $H^\pm \to \tau^\pm\nu_\tau$ and $H^\pm \to tb$ channels. The decay channel $H^\pm \to W^\pm h^0$ is vanishing because $H^\pm W^\mp h^0$ coupling is proportional to $\cos(\beta-\alpha) \approx 0$. In 2HDM type X, the coupling $H^\pm\tau^\mp\nu_\tau$ is proportional to $\tan\beta$ and since we assume that $\tan\beta \geq 2.5$, the $\tau\nu_\tau$ channel is slightly larger than in the 2HDM type I. It is clear from the lower panels of Fig. 2 that before the $W^\pm A^0$ threshold, $H^\pm \to \tau^\pm\nu_\tau$ is the dominant decay mode and it is amplified by taking large $\tan\beta$. In fact, such a large $\tan\beta$ not only enhances the $\tau\nu_\tau$ channel but also reduces $H^\pm \to cb, cs, tb$ modes, which are all proportional to $\cot\beta$. After crossing $W^\pm A^0$ threshold, $H^\pm \to W^\pm A^0$ becomes the dominant decay mode and taking large $\tan\beta$ can further suppress $H^\pm \to tb$ and makes $H^\pm \to W^\pm A^0$ even larger. Note that in the alignment limit $\cos(\beta-\alpha) = 0$, the coupling $H^\pm W^\mp h^0$ vanishes while $H^\pm W^\mp H^0$ is maximal and becomes similar to $H^\pm W^\mp A^0 = g/2$. Therefore, if $H^\pm \to W^\mp H^0$ is kinematically open it will compete on equal footing with $H^\pm \to W^\pm A^0$.

If $\tan\beta$ increases beyond 20 (45), the $\tau\nu$ mode could become comparable to the WA

mode for $m_{H^\pm} \gtrsim 200$ GeV and $m_{A^0} = 100$ (65) GeV in type-X. In such a case, the model would be subject to the current charged Higgs searches via the $\tau\nu$ mode. In the following, we will concentrate on a scenario in which the WA is the dominant mode.

The branching fractions for A^0 are depicted in Fig.3 as a function of $\tan\beta$ for $m_{A^0} = 65$ GeV in 2HDM type-I (left panel) and type-X (right panel). In 2HDM type I, all couplings $A^0 ff$ are proportional to $\cot\beta$. Therefore, the $\tan\beta$ factorizes out in the branching ratio calculation leading to constant $B(A^0 \to b\bar{b}, \tau^+\tau^-, \mu^+\mu^-)$ as a function of $\tan\beta$. In the case of type X, the branching ratios $B(A^0 \to \tau^+\tau^-, \mu^+\mu^-)$ are enhanced for large $\tan\beta$ while $B(A^0 \to b\bar{b})$ is suppressed. Note for $m_{A^0} = 100$ GeV, none of $A^0 \to Z^* h^0$ and $A^0 \to W^{\mp *} H^\pm$ are open, we observe similar behavior for $B(A^0 \to f\bar{f})$ in both type I and X.

2. *LHC Constraint from $t \to bH^+ \to b\tau\nu_\tau$*

For direct searches the LEP collaborations [6] had searched for charged Higgs pair production via the Drell-Yan process $e^+e^- \to Z/\gamma \to H^+H^-$, excluding $M_{H^\pm} < 80$ GeV (Type-II) and $M_{H^\pm} < 72.5$ GeV (Type-I) at 95% confidence level. The LHC collaborations also reported their charged Higgs search results for various mass regions. In the low mass region, the main decay mode is via $t \to bH^+$ followed by $H^\pm \to \tau^\pm\nu_\tau$ from CMS [11, 12] and ATLAS [8, 9]. In the high mass region, the main decay mode is $H^+ \to t\bar{b}$ from CMS [11, 17] and ATLAS [39].

When the charged Higgs mass is below $m_t - m_b$, it can be abundantly produced in top-quark decays, $t \to bH^+$, followed by charged Higgs decay $H^+ \to \tau^+\nu_\tau$ or $H^+ \to W^+A^0$. The CMS search for $t \to bH^+ \to b(\tau^+\nu_\tau)$ [11–13] set limits on $B(t \to bH^+) \times B(H^+ \to \tau^+\nu_\tau)$. We rescale their limits to the type I and X 2HDM's and show the exclusions in $(m_{H^\pm}, \tan\beta)$ plane. We note that in type I and X the decay width of $t \to bH^+$ scales as $\cot^2\beta$:

$$\Gamma(t \to bH^+) = \frac{G_F}{8\sqrt{2}\pi}\frac{|V_{tb}|^2}{m_t}\lambda^{1/2}\left(1, \frac{m_b^2}{m_t^2}, \frac{m_{H^\pm}^2}{m_t^2}\right) \times \left[(m_t^2 + m_b^2)\cot^2\beta(m_t^2 + m_b^2 - m_{H^\pm}^2) - 4m_t^2 m_b^2 \cot^2\beta\right] . \quad (8)$$

where $\lambda^{1/2}(1, x^2, y^2) \equiv \sqrt{[1-(x+y)^2][1-(x-y)^2]}$.

Interpretation of the CMS exclusion region [11–13] in the framework of 2HDM type I and X in $(\tan\beta, m_{H^\pm})$ plane is illustrated in Fig. 4 for both cases: $H^\pm \to W^\pm A^0$ closed and

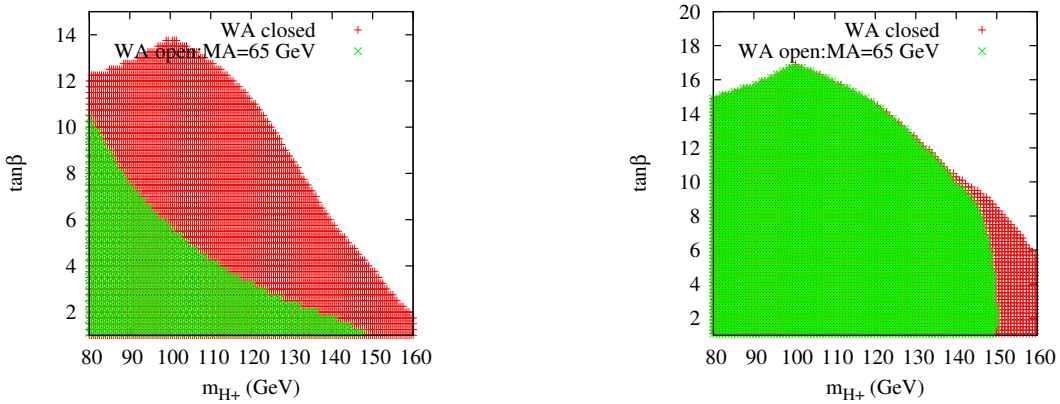

FIG. 4. Interpretation of CMS exclusion regions [11–13] in the 2HDM type I (left panel) and type X (right panel) projected on the plane of $(m_{H^\pm}, \tan\beta)$. The red points stand for the case the WA mode is closed while the green points are for the case that the WA mode is open, with $m_{A^0} = 65$ GeV.

$H^\pm \to W^\pm A^0$ open.[3] It is clear that for charged Higgs mass ≤ 120 GeV with the $W^\pm A^0$ channel closed, $\tan\beta \leq 12$ is excluded. This exclusion is reduced for $m_{H^\pm} \geq 120$ GeV due to the fact that $B(H^+ \to \tau^+\nu_\tau)$ is highly suppressed for 2HDM type I as $\tan\beta$ increases. On the other hand, when the WA mode is open, the exclusion region in $(\tan\beta, m_{H^\pm})$ plane is significantly reduced in 2HDM type I. In the case of 2HDM type X, one can see from the right panel that $\tan\beta \leq 6$ is excluded for any value of charged Higgs mass provided that $H^\pm \to W^\pm A^0$ is closed. This limit on $\tan\beta$ is slightly more severe than what we can get from flavor physics (see the above discussion). When $H^\pm \to W^\pm A^0$ is open, starting from $m_{H^\pm} \geq 145$ GeV for $m_{A^0} = 65$ GeV, $H^\pm \to \tau\nu_\tau$ mode is suppressed leading to no exclusion for any $\tan\beta$. Below the $W^\pm A^0$ threshold, $H^\pm \to \tau\nu_\tau$ channel is still the dominant one, one can see that the green exclusion completely overlaps with the red one in 2HDM X.

3. LHC Constraint from $t \to bH^+ \to bW^+A^0 \to bW^+\mu^+\mu^-$

Recently, the CMS collaboration [25] also reported the direct search for light charged Higgs via $t \to bH^+ \to b(W^+A^0) \to b(l^+\nu_l)(\mu^+\mu^-)$ with $l = e, \mu$ [25] assuming that $H^\pm$ decays 100% into $W^\pm A^0$ and $B(A^0 \to \mu^+\mu^-) = 3 \times 10^{-4}$ and set a limit on $B(t \to bH^+)$.

[3] Here the results presented in Fig. 4 are consistent with the Fig.3 of Ref. [40], in which the WA mode was not considered.

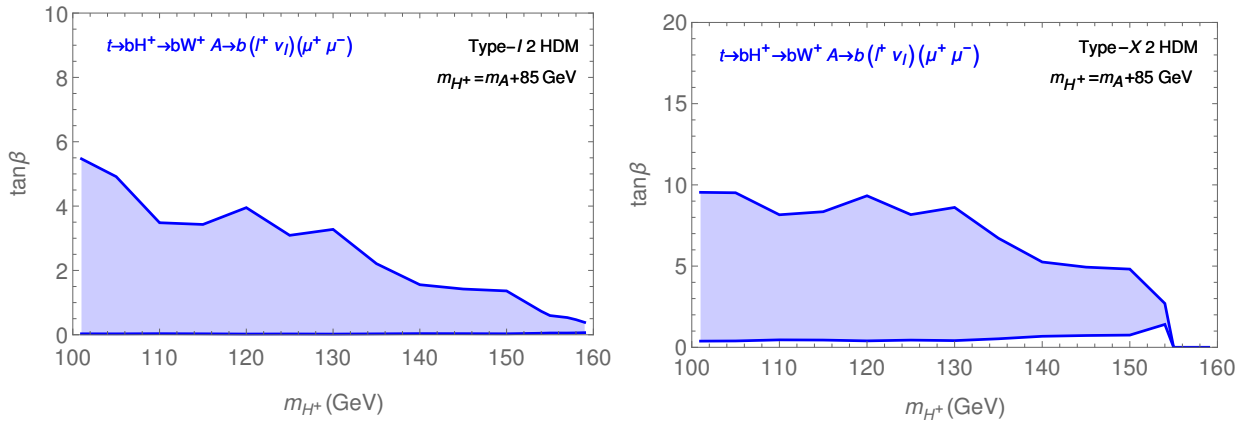

FIG. 5. Exclusions in the parameter space of $(m_{H^\pm}, \tan\beta)$ for type I (left panel) and for type X (right panel) 2HDM's obtained by rescaling the observed limits of the CMS results in Refs. [25] based on $t \to bH^+ \to bW^+A \to b(l^+\nu_l)(\mu^+\mu^-)$.

We rescale the CMS limit and interpret it for 2HDM type I and X, which are depicted in Fig. 5. It is clear that the exclusion based on $A^0 \to \mu^+\mu^-$ also shows some differences between type I and X. It is easy to see from Fig. 3 that $B(A^0 \to \mu^+\mu^-)$ is only about 2×10^{-4} in type I but is as large as 3×10^{-3} in type X for $\tan\beta > 3$. Therefore, the excluded region (blue shaded) in Fig. 5 for type X is much larger than that of type I.

In the rest of this work, we focus on type I and X 2HDM's, in which the charged Higgs mass is much less restricted. In addition, we also focus on the currently-allowed parameter space region where $H^\pm$ decays dominantly into $W^\pm A^0$ via VBF production of same-sign charged Higgs boson pair. This is complementary to the study in Ref. [26].

Before moving to the next section, we make some comments for direct searches of light H^0 and A^0 at the LHC. In the (near) alignment limit, only fermionic production channels $gg \to H^0/A^0$, $pp \to t\bar{t}H^0/A^0$ and $pp \to b\bar{b}H^0/A^0$ with decay modes $H^0/A^0 \to b\bar{b}, \tau^+\tau^-, \mu^+\mu^-$ and $\gamma\gamma$ are possible to directly detect light H^0 and A^0 [41–44]. [4] In type I and X 2HDM's, all of these production channels are proportional to $\cot^2\beta$. Therefore, it is rather challenging to detect both of them for large $\tan\beta$. Besides, it is also hard to distinguish between the CP properties of light H^0 and A^0 at the LHC, even if we already observe two different resonance

[4] The most stringent constraint from the direct search of light pseudoscalar $A^0 \to \tau^+\tau^-$ at the LHC comes from Ref. [42]. If we take $\tan\beta = 3$ for Type-I and X 2HDMs, and compare the constraints from Ref. [42] for the process $pp \to b\bar{b}A^0$ with $A^0 \to \tau^+\tau^-$, then the cross sections for Type-I (Type-X) are about 3 (2) orders smaller than the current constraints for $25 < m_{A^0} < 70$ GeV. Therefore, we will ignore these constraints in our study.

peaks from their fermionic channels. Based on these difficulties, we argue that the process in Eq. 1 can be another way to double check the mass splitting Δm between H^0 and A^0.

Note that the case of relatively light CP-odd ($m_A < 60$ GeV) is now rather severely constrained by LHC searches. Several dedicated searches can be used to constraint such scenario. The first search is $pp \to h^0 \to A^0 A^0 \to 4f$ [45–49] which is performed both by ATLAS and CMS and the second one is $pp \to H^0 \to Z A^0 \to 2bl^+l^-$ [50]. Even though the $h^0 A^0 A^0$ coupling can be adjusted to be very small by tuning the parameter m_{12}^2, this m_{12}^2 may also violate theoretical and EWPT constraints as well, especially for large mass splitting between H^0 and A^0. In this regards, we perform a global scan for the benchmark point $m_{A^0} \in [15-60]$ GeV with $0.97 \leq \sin(\beta-\alpha) \leq 1$ by using the public softwares 2HDMC, **HiggsBounds** [51] and **Higgssignal** [52]. For such light CP-odd, h^0 can decay with a significant branching ratio into $A^0 A^0$. In addition, the heavy CP-even H^0 can also decay dominantly into $A^0 Z$ because $H^0 A^0 Z$ coupling being proportional to $\sin(\beta-\alpha) \approx 1$. However, we found that the allowed parameter space that survive to the theoretical and EWPT constraints is now almost excluded either by $pp \to h^0 \to A^0 A^0 \to \{b\bar{b}b\bar{b}, \mu^+\mu^- b\bar{b}, \mu^+\mu^-\tau^+\tau^-, b\bar{b}\tau^+\tau^-\}$ [45–49] or by $pp \to H^0 \to A^0 Z \to b\bar{b}l^+l^-$ [50] searches.

IV. SAME-SIGN CHARGED HIGGS PAIR PRODUCTION

A. The behavior of $pp \to H^\pm H^\pm j_F j_F$ process

Recently, the novel process of same-sign charged Higgs pair production was proposed in Ref. [26], and especially this process is very sensitive to the mass splitting $\Delta m \equiv m_{H^0} - m_{A^0}$ in the 2HDMs as it will be shown below. The cross section is enhanced according to the large mass splitting Δm. This process can be generated via the same-sign W boson fusion, $pp \to W^{\pm *} W^{\pm *} j_F j_F \to H^\pm H^\pm j_F j_F$ at hadron colliders, where j_F denotes the forward and energetic jet directly from the initial parton.

The relation between the mass splitting Δm and same-sign charged Higgs pair production can be understood in the $2 \to 2$ subprocess $W^+W^+ \to H^+H^+$ at amplitude level. This subprocess is induced by three t-channel diagrams with h^0, H^0 and A^0 exchange. In the alignment limit, $\cos(\beta-\alpha) = 0$, which is favored by the current Higgs data, the scattering

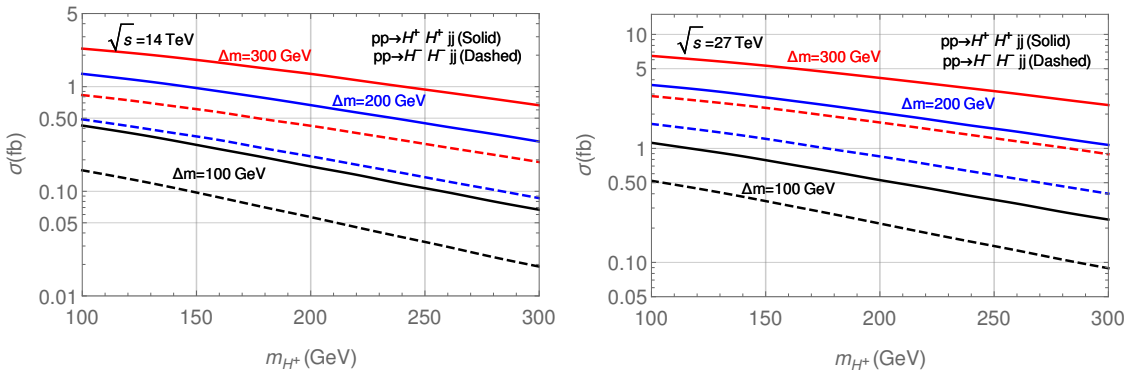

FIG. 6. The production cross sections of $pp \to H^+H^+j_Fj_F$ (solid line) and $pp \to H^-H^-j_Fj_F$ (dashed line) versus $m_{H^\pm}$ at $\sqrt{s} = 14$ TeV (left panel) and $\sqrt{s} = 27$ TeV (right panel), for Δm =100 GeV (black), 200 GeV (blue), and 300 GeV (red). Notice the VBF cut $\eta_{j_1} \times \eta_{j_2} < 0$ and $|\Delta\eta_{jj}| > 2.5$ for the minimum rapidity difference between the forward jet pair are applied.

amplitude for

$$W^+(p_1)W^+(p_2) \to H^+(q_1)H^+(q_2)$$

is only mediated by H^0 and A^0 and is given by

$$\begin{aligned} i\mathcal{M}^{H^0+A^0} &= ig^2 q_1\cdot\epsilon(p_1)\; q_2\cdot\epsilon(p_2)\; \left[\frac{1}{t-m^2_{A^0}} - \frac{1}{t-m^2_{H^0}}\right] \;+\; (q_1 \leftrightarrow q_2, t \leftrightarrow u) \\ &\propto \Delta m \times \frac{m_{H^0}+m_{A^0}}{(t-m^2_{H^0})(t-m^2_{A^0})}\; q_1\cdot\epsilon(p_1)\; q_2\cdot\epsilon(p_2) \;+\; (q_1 \leftrightarrow q_2, t \leftrightarrow u) \end{aligned} \tag{9}$$

where $t = (p_1 - q_1)^2$ and $u = (p_1 - q_2)^2$, and $\epsilon(p_{1,2})$ are the polarization 4-vectors of the incoming W^+ bosons. As it can be seen, the above amplitude is proportional to Δm.

As indicated by Eq. (9) the production cross section of $pp \to H^\pm H^\pm j_F j_F$ scales as the square of the mass splitting Δm. We quantitatively show this relation by plotting the production cross sections versus $m_{H^\pm}$ in Fig. 6 with Δm = 100, 200, and 300 GeV at $\sqrt{s} = 14$ TeV (left panel) and $\sqrt{s} = 27$ TeV (right panel). It is clear to observe that the cross section is enhanced according to the large mass splitting Δm. Note that we have used the general Two-Higgs-Doublet Model UFO model file [53] and employ **Madgraph5 aMC@NLO** [54] with VBF cut $\eta_{j_1} \times \eta_{j_2} < 0$ and $|\Delta\eta_{jj}| > 2.5$ for the minimum rapidity difference between the forward jet pair to evaluate the cross sections. Furthermore, in order to study the effects of the near-alignment limit on the production cross sections, we list some benchmark points for the relation of cross sections with $\sin(\beta-\alpha) = 1, 0.95, 0.9$ in Table II at $\sqrt{s} = 14$ TeV and Table III at $\sqrt{s} = 27$ TeV, respectively.

TABLE II. Sum of cross sections for $\sigma(pp \to H^+H^+j_Fj_F)$ and $\sigma(pp \to H^-H^-j_Fj_F)$ [fb] at $\sqrt{s} = 14$ TeV for $\sin(\beta-\alpha) = 1, 0.95, 0.9$ with the benchmark points $\Delta m = 100, 200, 300$ GeV and $m_{H^\pm} = 100, 200, 300$ GeV. Notice the VBF cut $\eta_{j_1} \times \eta_{j_2} < 0$ and $|\Delta\eta_{jj}| > 2.5$ for the minimum rapidity difference between the forward jet pair have been applied.

		$\sigma(pp \to H^\pm H^\pm j_F j_F)$ [fb]		
Δm (GeV)	$m_{H^\pm}$ (GeV)	$\sin(\beta-\alpha) = 1$	$\sin(\beta-\alpha) = 0.95$	$\sin(\beta-\alpha) = 0.9$
100	100	5.84×10^{-1}	5.43×10^{-1}	5.03×10^{-1}
	200	2.30×10^{-1}	2.11×10^{-1}	1.95×10^{-1}
	300	8.57×10^{-2}	7.86×10^{-2}	7.21×10^{-2}
200	100	1.81	1.59	1.39
	200	8.82×10^{-1}	7.66×10^{-1}	6.62×10^{-1}
	300	3.85×10^{-1}	3.33×10^{-1}	2.85×10^{-1}
300	100	3.14	2.70	2.32
	200	1.75	1.49	1.26
	300	8.54×10^{-1}	7.21×10^{-1}	6.05×10^{-1}

We stress first that the production cross section $pp \to H^\pm H^\pm j_F j_F$ is the same for both 2HDM type I and X. Only the decay of the charged Higgs bosons that will make the process model dependent. The full signal process including decays of $H^\pm$, $W^\pm$, A^0 is given by

$$pp \to W^{\pm *}W^{\pm *}j_Fj_F \to H^\pm H^\pm j_Fj_F \to (W^\pm A^0)(W^\pm A^0)j_Fj_F \to l^\pm\nu_l(b\bar{b})l^\pm\nu_l(b\bar{b})j_Fj_F \tag{10}$$

in type-I 2HDM, and

$$pp \to W^{\pm *}W^{\pm *}j_Fj_F \to H^\pm H^\pm j_Fj_F \to (W^\pm A^0)(W^\pm A^0)j_Fj_F \to l^\pm\nu_l(\tau^+\tau^-)l^\pm\nu_l(\tau^+\tau^-)j_Fj_F \tag{11}$$

in type-X 2HDM. We advocate that the novel signatures including the combination of a pair of same-sign dileptons ($l^\pm l^\pm$), a forward and energetic jet pair (j_Fj_F), and two pairs of bottom quarks ($b\bar{b}$) or tau leptons ($\tau^+\tau^-$) coming from two light pseudoscalars A^0 can largely reduce the possible SM backgrounds.

TABLE III. Sum of cross sections for $\sigma(pp \to H^+H^+j_Fj_F)$ and $\sigma(pp \to H^-H^-j_Fj_F)$ [fb] at $\sqrt{s} = 27$ TeV for $\sin(\beta-\alpha) = 1, 0.95, 0.9$ with the benchmark points $\Delta m = 100, 200, 300$ GeV and $m_{H^\pm} = 100, 200, 300$ GeV. Notice the VBF cut $\eta_{j_1} \times \eta_{j_2} < 0$ and $|\Delta\eta_{jj}| > 2.5$ for the minimum rapidity difference between the forward jet pair have been applied.

		$\sigma(pp \to H^\pm H^\pm j_F j_F)$ [fb]		
Δm (GeV)	$m_{H^\pm}$ (GeV)	$\sin(\beta-\alpha) = 1$	$\sin(\beta-\alpha) = 0.95$	$\sin(\beta-\alpha) = 0.9$
100	100	1.64	1.52	1.41
	200	7.46×10^{-1}	6.87×10^{-1}	6.34×10^{-1}
	300	3.26×10^{-1}	2.99×10^{-1}	2.75×10^{-1}
200	100	5.24	4.59	4.00
	200	2.91	2.53	2.18
	300	1.47	1.27	1.09
300	100	9.35	8.04	6.87
	200	5.84	4.97	4.20
	300	3.29	2.77	2.33

Even in case that the masses of H^0 and A^0 are separated wide enough and they can be directly measured from other production channels, the current VBF process is still worthwhile to search for. First, the advantage of this process is that it does not depend on Yukawa couplings, in contrast to direct searches of H^0, A^0, or $H^\pm$. The cross section of the this process is a function of mainly $m_{H^\pm}$, ΔM in the limit $\sin(\beta-\alpha) = 1$. Therefore, if no such process is observed, it can exclude the charged Higgs mass or mass correlation between m_{H^0} and m_{A^0}. Second, since H^0 is difficult to be discovered in the (near) alignment limit ($\sin(\beta-\alpha) \approx 1$) in type-I or type-X 2HDM, this process can imply the mass of H^0. Nevertheless, this is only true in 2HDMs. If the light boson A^0 can be discovered in the near future, the usefulness of this process is to tell the mass difference between H^0 and A^0 even we do not find the heavier boson H^0. On the other hand, if both H^0 and A^0 have been discovered, the usefulness of this process is to tell if the cross section matches the prediction in 2HDM.

TABLE IV. Cut flow table for the Type-I 2HDM signal $pp \to H^{\pm}H^{\pm}j_F j_F$ with $m_{H^{\pm}} = 205$ GeV, $m_{A^0} = 65$ GeV, $\Delta m = 200$ GeV, $\tan\beta = 5$ and $\sin(\beta-\alpha) = 0.97$, and various backgrounds at $\sqrt{s} = 14$ TeV.

Cross section (fb)	signal	$t\bar{t}t\bar{t}$	$t\bar{t}b\bar{b}l^+l^-$	$3t1b$	$2t2b2j$
Preselection	2.07×10^{-2}	4.94×10^{-2}	1.08×10^{-2}	7.74×10^{-5}	8.29×10^{-5}
$N(b,l^{\pm}) \geq 3,2,$ $P_T^{b,l^{\pm}} > 20$GeV,$\lvert\eta^{b,l}\rvert < 2.5$	1.76×10^{-3}	6.17×10^{-3}	9.56×10^{-4}	9.57×10^{-6}	9.81×10^{-6}
$N(j) \geq 2,$ $P_T^{j} > 30$GeV,$M_{jj} > 500$GeV	1.46×10^{-3}	5.15×10^{-3}	4.18×10^{-4}	2.88×10^{-6}	4.05×10^{-6}
$m_{H^{\pm}}$ Cuts $M_{bbl^{\pm}} < 250$GeV	1.41×10^{-3}	3.50×10^{-3}	2.71×10^{-4}	1.85×10^{-6}	2.62×10^{-6}
m_A Cuts $50 < M_{bb} < 90$GeV	1.30×10^{-3}	1.68×10^{-3}	1.61×10^{-4}	7.58×10^{-7}	1.14×10^{-6}

B. Signal-background analysis for Type-I 2HDM

The signal process in Eq. (10) is unique with a signature including the combination of a pair of same-sign dileptons ($l^{\pm}l^{\pm}$), a pair of forward and energetic jets ($j_F j_F$), and two pairs of bottom quarks ($b\bar{b}$) coming from two light pseudoscalar A^0. There are a few SM backgrounds that can mimic this kind of final states. We consider the following four processes as the main SM backgrounds,

$$pp \to t\bar{t}t\bar{t} \to (bW^+)(\bar{b}W^-)(bW^+)(\bar{b}W^-) \to l^{\pm}l^{\pm}4b4j, \tag{12}$$

$$pp \to t\bar{t}b\bar{b}l^+l^- \to (bW^+)\bar{b}(\bar{b}W^-)bl^+l^- \to l^{\pm}l^+l^-4b2j, \tag{13}$$

$$\begin{aligned} & pp \to t\bar{t}t\bar{b} \to (bW^+)(\bar{b}W^-)(bW^+)\bar{b} \to l^+l^+4b2j \\ or \quad & pp \to t\bar{t}\bar{t}b \to (bW^+)(\bar{b}W^-)(\bar{b}W^-)b \to l^-l^-4b2j, \end{aligned} \tag{14}$$

$$\begin{aligned} & pp \to tt\bar{b}\bar{b}jj \to (bW^+)(bW^+)\bar{b}\bar{b}jj \to l^+l^+4b2j \\ or \quad & pp \to \bar{t}\bar{t}bbjj \to (\bar{b}W^-)(\bar{b}W^-)bbjj \to l^-l^-4b2j\,. \end{aligned} \tag{15}$$

All signal and SM background events are simulated at leading order (LO) using Madgraph5 aMC@NLO. [5] In the following, we choose $m_{H^\pm} = 205$ GeV and $m_{A^0} = 65$ GeV to illustrate the cut flow under a sequence of selection cuts at $\sqrt{s} = 14$ TeV.

1. We first identify the forward jet pair ($j_F j_F$) in the VBF-type process and apply the VBF cut $\eta_{j_1} \times \eta_{j_2} < 0$ and $|\Delta\eta_{jj}| > 2.5$ for the minimum rapidity difference between the forward jet pair in Madgraph5 aMC@NLO at parton level for all signal and SM background events. The cross sections for both signal and background events after this pre-selection cut are shown in the first row of Table IV.

2. Then we employ **Pythia8** [55] for parton showering and hadronization. **Delphes3** [56] with default settings is used for fast detector simulation. [6] Finally, all events are analyzed with **MadAnalysis5** [57]. We require to see a pair of same-sign dileptons ($l^\pm l^\pm$) and at least $3b$ in the event as the trigger with the following sequence of event selection cuts

$$N(b, l^\pm) \geq 3, 2, \quad P_T^{l^\pm} > 20 \text{ GeV}, \quad |\eta^{l^\pm}| < 2.5, \quad P_T^b > 20 \text{ GeV}, \quad |\eta^b| < 2.5. \tag{16}$$

   The b-jets are selected with the efficiency as a function of P_T as, $\epsilon_b = 0.85 \times \tanh(0.0025 \times P_T) \times (25.0/(1 + 0.063 \times P_T))$ and the misidentification rate from c-jets and light jets to b-jets are $P(c \to b) = 0.25 \times \tanh(0.018 \times P_T) \times (1/(1 + 0.0013 \times P_T))$ and $P(j \to b) = 0.01 + 0.000038 \times P_T$, separately. The cross sections for both signal and background events are shown in the second row of Table IV.

3. The forward jet pair is also required to be energetic with the following selection cuts

$$N(j) \geq 2, \quad p_T^j > 30 \text{ GeV}, \quad |\eta^j| < 5, \quad m_{jj} > 500 \text{ GeV}. \tag{17}$$

   The cross sections after this step for both signal and background events are shown in the third row of Table IV.

[5] The NLO QCD corrections for the signal process in Eq. (10) and background processes in Eq. (12) and (13) have been checked with Madgraph5 aMC@NLO. We assume that the kinematic distributions are only mildly affected by these higher order QCD effects.

[6] Notice that we apply the Delphes 3.4.1 in the Madgraph5 aMC@NLO. Comparing with the HL-LHC Delphes card in the most current version Delphes 3.4.2, they added the conditions $|\eta| < 2.5$ and $10 < P_T < 1000$ GeV for the same τ-tagging efficiency and light jet to tau-jet misidentification rate. On the other hand, they also included the η dependence with similar P_T dependence settings compared with our default version. We expect these changes will only make very mild modifications of our conclusions.

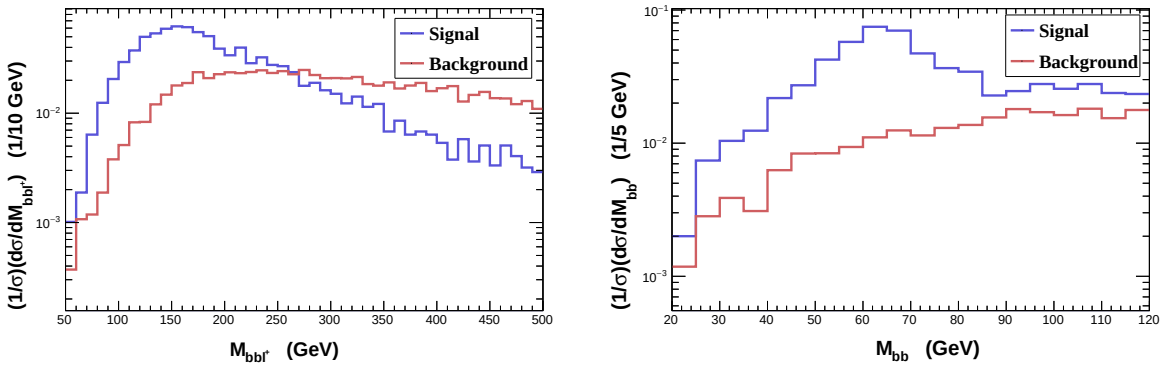

FIG. 7. Invariant mass distributions of $M_{bbl^\pm}$ (left panel) and M_{bb} (right panel) for the signal with $m_{H^\pm} = 205$ GeV, $m_{A^0} = 65$ GeV, $\Delta m = 200$ GeV, $\tan\beta = 5$ and $\sin(\beta - \alpha) = 0.97$, and the total background at $\sqrt{s} = 14$ TeV. Preselection cuts in Eqs. (16) and (17) are imposed.

4. The kinematical distributions of $M_{bbl^\pm}$ and M_{bb} with $m_{H^\pm} = 205$ GeV and $m_{A^0} = 65$ GeV for the signal and backgrounds are shown in Fig. 7. Note that we have applied all the selection cuts except for $m_{H^\pm}$ and m_{A^0} cuts in these two kinematical distributions. The signal distribution of $M_{bbl^\pm}$ tends to concentrate in the region of $M_{bbl^\pm} < 250$ GeV and decreases more rapidly toward the higher $M_{bbl^\pm}$. On the other hand, the background is relatively flat after 150 GeV to 500 GeV. It is also clear to observe the peak shape at 65 GeV in M_{bb} distribution for the signal from the resonance of A^0. These two behaviors can help us to distinguish between the signal and the background.

5. Finally, in order to further reduce the contributions from SM backgrounds, the following selection cuts are imposed on both signal and background events. For $m_{H^\pm}$ cuts at least two bottom quarks and a lepton have to satisfy

$$M_{bbl^\pm} \leq M_{H^\pm} + 45 \text{ GeV}. \tag{18}$$

For m_{A^0} cuts at least a pair of bottom quarks are required to be around the mass of A^0:

$$m_{A^0} - 15 \text{ GeV} \leq M_{bb} \leq m_{A^0} + 25 \text{ GeV}. \tag{19}$$

Again, the cross sections for both signal and background events after this sequence of event selection cuts are shown in the last two rows of Table IV.

TABLE V. Cut flow table for the Type-I 2HDM signal $pp \to H^{\pm}H^{\pm}j_F j_F$ with $m_{H^{\pm}} = 205$ GeV, $m_{A^0} = 65$ GeV, $\Delta m = 200$ GeV, $\tan\beta = 5$ and $\sin(\beta-\alpha) = 0.97$, and various backgrounds at $\sqrt{s} = 27$ TeV.

Cross section (fb)	signal	$t\bar{t}t\bar{t}$	$t\bar{t}b\bar{b}l^+l^-$	$3t1b$	$2t2b2j$
Preselection	6.88×10^{-2}	5.67×10^{-1}	5.60×10^{-2}	2.40×10^{-4}	6.76×10^{-4}
$N(b, l^{\pm}) \geq 3, 2$, $P_T^{b,l^{\pm}} > 20$GeV,$\lvert\eta^{b,l}\rvert < 2.5$	5.15×10^{-3}	5.67×10^{-2}	4.43×10^{-3}	2.44×10^{-5}	6.42×10^{-5}
$N(j) \geq 2$, $P_T^j > 30$GeV,$M_{jj} > 500$GeV	4.54×10^{-3}	5.22×10^{-2}	2.49×10^{-3}	9.67×10^{-6}	3.27×10^{-5}
$m_{H^{\pm}}$ Cuts					
$M_{bbl^{\pm}} < 200$GeV	4.10×10^{-3}	2.28×10^{-2}	1.08×10^{-3}	4.29×10^{-6}	1.45×10^{-5}
m_A Cuts					
$50 < M_{bb} < 80$GeV	3.76×10^{-3}	1.12×10^{-2}	6.09×10^{-4}	1.91×10^{-6}	7.15×10^{-6}

After all selection cuts the signal-to-background ratio is almost close to 1. With a luminosity of 3000 fb^{-1} we expect about 4 signal and 5 background events. The major background comes from $t\bar{t}t\bar{t}$ production while the other backgrounds listed in Table IV are much suppressed.

Even though the signal-to-background ratio is close to one for the analysis at the HL-LHC, the total number of events is small and the fluctuations of SM backgrounds may also be an issue. Since we cannot draw any concrete conclusion for this situation, we further extend the signal-background analysis to the proposed 27 TeV pp collider(HE-LHC). The SM background cross sections grow faster than the signal one from $\sqrt{s} = 14$ to 27 TeV. In order to reduce the enhanced background cross sections, both $m_{H^{\pm}}$ and m_{A^0} cuts are tightened relative to those in Eqs. (18) and (19). For $m_{H^{\pm}}$ cuts at least two bottom quarks and a lepton have to satisfy

$$M_{bbl^{\pm}} \leq M_{H^{\pm}} - 5 \text{ GeV}. \tag{20}$$

For m_{A^0} cuts at least a pair of bottom quarks is required to be around the mass of A^0:

$$|M_{bb} - m_A| \leq 15 \text{ GeV}. \tag{21}$$

Other preselection cuts, given in Eqs. (16) and (17), are the same as before. On the other hand, the shape of kinematical distributions for $M_{bbl^{\pm}}$ and M_{bb} with $m_{H^{\pm}} = 205$ GeV and

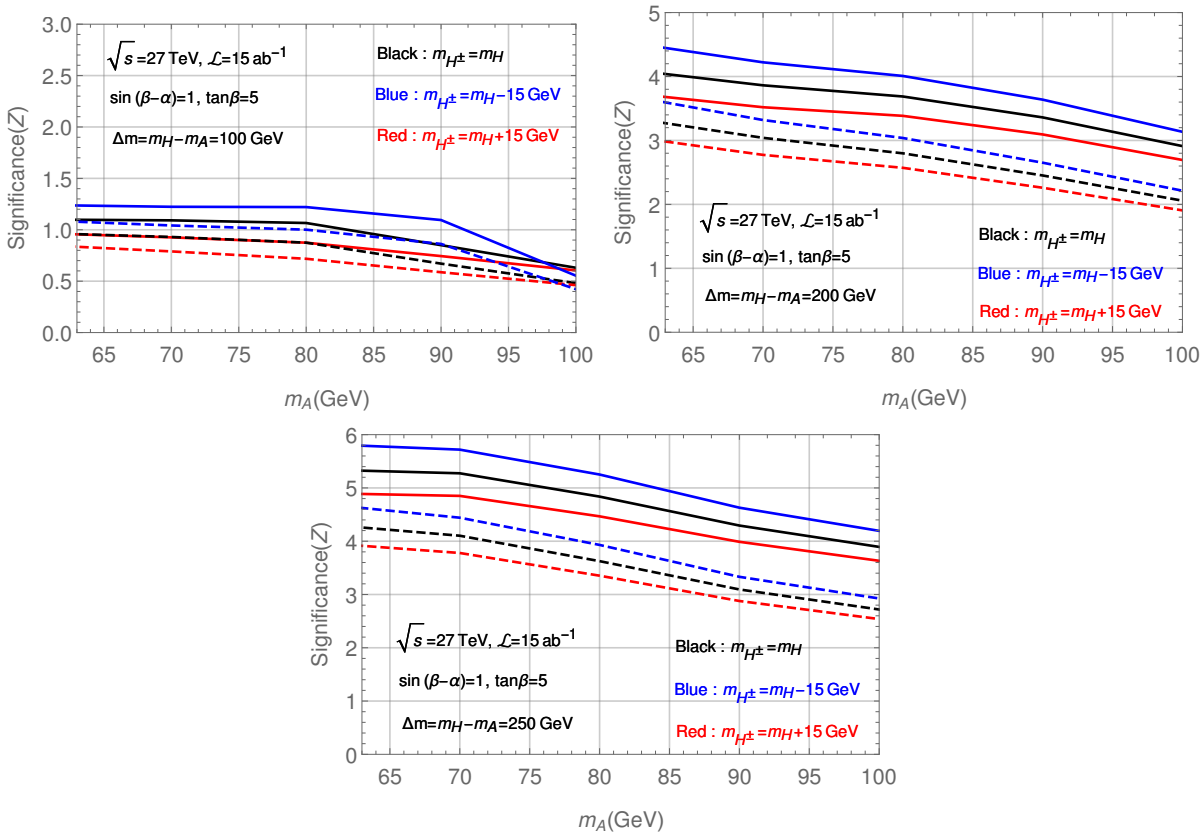

FIG. 8. The significance Z versus m_{A^0} from 63 to 100 GeV in Type-I 2HDM at $\sqrt{s} = 27$ TeV with luminosity $\mathcal{L} = 15\,\text{ab}^{-1}$. We have fixed $\sin(\beta-\alpha) = 1$ and $\tan\beta = 5$ with $\Delta m \equiv m_{H^0} - m_{A^0} = 100$ GeV (upper-left panel), 200 GeV (upper-right panel), and 250 GeV (lower panel). The dashed lines correspond to additional 5% systematic uncertainties of the SM background events in Eq. (23).

$m_{A^0} = 65$ GeV at $\sqrt{s} = 27$ TeV for the signal and backgrounds are similar to Fig. 7, so we do not repeat displaying them here. We choose the same signal benchmark point to illustrate the cut flow under a sequence of selection cuts at $\sqrt{s} = 27$ TeV in Table V.

Finally, we summarize our signal-background analysis for Type-I 2HDM at $\sqrt{s} = 27$ TeV with luminosity $\mathcal{L} = 15ab^{-1}$ in Fig. 8. The preselection cuts in Eqs. (16), (17), (20) and (21) are imposed as before. We vary m_{A^0} from 63 to 100 GeV with fixed $\sin(\beta-\alpha) = 1$ and $\tan\beta = 5$ for $\Delta m = m_{H^0} - m_{A^0} = 100$ GeV (upper-left panel), 200 GeV (upper-right panel), and 250 GeV (lower panel) in Fig. 8 as the illustrative examples. The black lines are $m_{H^\pm} = m_{H^0}$, the blue lines are $m_{H^\pm} = m_{H^0} - 15$ GeV, and the red lines are $m_{H^\pm} = m_{H^0} + 15$ GeV. We first define the significance by

$$Z = \sqrt{2 \cdot [(s+b) \cdot ln(1+s/b) - s]}\,, \tag{22}$$

where s and b represent the numbers of signal and background events, respectively. According to the production cross sections of same-sign charged Higgs in the right panel of Fig. 6, it is obvious that the cases with moderate mass splittings Δm are difficult to be detected even at HE-LHC with high luminosities. The maximum significance is only about $Z = 1.2$ for $\Delta m = 100$ GeV. We need other charged Higgs production channels to detect this kind of moderate mass splitting Δm cases. However, this same-sign charged Higgs production channel is sensitive to the cases with large mass splitting Δm. The average significance is about $Z = 3.5$ for m_{A^0} from 63 GeV to 100 GeV with $\Delta m = 200$ GeV, and its maximum can reach to more than $Z = 4.4$ at $m_{A^0} = 63$ GeV. Moreover, the average significance can grow to about $Z = 4.5$ for m_{A^0} from 63 GeV to 100 GeV with $\Delta m = 250$ GeV, and its maximum can further reach to $Z = 5.8$ for $m_{A^0} \leq 70$ GeV.

We further consider a 5% systematic uncertainty in estimation of the SM background. The significance of the signal is modified to

$$Z = \sqrt{2 \cdot \left[(s+b) \cdot ln \left(\frac{(s+b)(b+\sigma_b^2)}{b^2 + (s+b)\sigma_b^2} \right) - \frac{b^2}{\sigma_b^2} \cdot ln \left(1 + \frac{\sigma_b^2 s}{b(b+\sigma_b^2)} \right) \right]}, \tag{23}$$

where σ_b is the systematic uncertainty of the SM background b. We show the effect of including systematic uncertainties as dashed lines in Fig. 8 for comparisons. [7] The reduction of the systematic uncertainty in future collider experiments is a long shot, but with better understanding of the SM backgrounds and theoretical calculations, a level of less than 10% systematic uncertainty is not beyond reach. If we take the number of signal and background events with the cross sections shown in the last row of Table V, $s = 56, b = 168$ with 15 ab^{-1} integrated luminosity. The significance $Z = 4.1$ with 0% systematic uncertainty, but reduces to 3.4, 2.4, 1.4 with 5%, 10%, 20% systematic uncertainties. Therefore, one can see that a systematic uncertainty better than 10% is needed to see a significant excess. In order to preserve a significant excess it is better to achieve as good as 5% systematic uncertainty.

C. Signal-background analysis for Type-X 2HDM

In type X 2HDM, the major decay of the pseudoscalar A^0 is $A^0 \to \tau\tau$. Therefore, we modify the above signal-background analysis to two pairs of tau leptons, instead of two pairs

[7] Notice that the 5% systematic uncertainty that we have assumed in estimation of the SM background is an optimistic choice. Even it is not trivial, this level of systematics might be still achievable at HE-LHC with luminosity $\mathcal{L} = 15ab^{-1}$.

TABLE VI. Cut flow table for the Type-X 2HDM signal $pp \to H^{\pm}H^{\pm}j_F j_F$ with $m_{H^{\pm}} = 205$ GeV, $m_{A^0} = 65$ GeV, $\Delta m = 200$ GeV, $\tan\beta = 5$ and $\sin(\beta-\alpha) = 0.97$, and various backgrounds at $\sqrt{s} = 14$ TeV.

Cross section (fb)	signal	$t\bar{t}Zjj$	$t\bar{t}W^{\pm}jj$	$W^{\pm}W^{\mp}Zjj$	$W^{\pm}ZZjj$
Preselection	2.98×10^{-2}	3.60×10^{-1}	2.44×10^{-1}	3.28×10^{-2}	1.87×10^{-3}
$N(\tau, l^{\pm}) \geq 3, 2$, $P_T^{\tau,l^{\pm}} > 20$GeV,$\lvert\eta^{\tau,l}\rvert < 2.5$	1.23×10^{-3}	7.42×10^{-3}	1.07×10^{-3}	3.89×10^{-4}	9.61×10^{-5}
$N(j) \geq 2$, $P_T^{j} > 30$GeV,$M_{jj} > 500$GeV	9.81×10^{-4}	4.63×10^{-3}	6.19×10^{-4}	1.97×10^{-4}	5.08×10^{-5}
b-jet veto	9.15×10^{-4}	1.15×10^{-3}	2.03×10^{-4}	1.71×10^{-4}	4.32×10^{-5}
$m_{H^{\pm}}$ Cut $M_{\tau^+\tau^- l^{\pm}} < 250$GeV	8.24×10^{-4}	7.52×10^{-4}	9.18×10^{-5}	1.15×10^{-4}	2.98×10^{-5}
m_{A^0} Cut $40 < M_{\tau^+\tau^-} < 100$GeV	7.95×10^{-4}	6.28×10^{-4}	5.81×10^{-5}	1.04×10^{-4}	2.73×10^{-5}

of bottom quarks, in the final state. The decay chain is shown in Eq. (11). Therefore, we are considering the following set of backgrounds at LO :

$$pp \to t\bar{t}Zjj \to (bW^+)(\bar{b}W^-)(\tau^+\tau^-)jj \to l^{\pm}2b3\tau 2j, \tag{24}$$

$$pp \to t\bar{t}W^{\pm}jj \to (bW^+)(\bar{b}W^-)(\tau^{\pm}\nu_{\tau})jj \to l^{\pm}2b2\tau 2j, \tag{25}$$

$$pp \to W^{\pm}W^{\mp}Zjj \to (l^{\pm}\nu_l)(\tau^{\mp}\nu_{\tau})(\tau^+\tau^-)jj \to l^{\pm}3\tau 2j, \tag{26}$$

$$pp \to W^{\pm}ZZjj \to (l^{\pm}\nu_l)(\tau^+\tau^-)(\tau^+\tau^-)jj \to l^{\pm}4\tau 2j\ . \tag{27}$$

The extra same-sign charged leptons may come from some cascade decays of the tau leptons, B mesons, or showering. Similarly, the extra tau leptons can also come from B meson cascade decays, showering, or jet misidentification.

Again, we choose $m_{H^{\pm}} = 205$ GeV and $m_{A^0} = 65$ GeV to illustrate the cut flow under a sequence of selection cuts.

1. We apply the same VBF cut $\eta_{j_1} \times \eta_{j_2} < 0$ and $|\Delta\eta_{jj}| > 2.5$ for the minimum rapidity difference between the forward jet pair at parton level for all signal and SM background events. Their cross sections after this pre-selection cut are shown in the first row of Table VI.

2. After parton showering and hadronization with Pythia8 and detector simulation by Delphes3, we apply the selections cuts for a pair of same-sign dileptons and at least 3τ:

$$N(\tau, l^{\pm}) \geq 3, 2, \quad P_T^{l^{\pm}} > 20 \text{ GeV}, \quad |\eta^{l^{\pm}}| < 2.5, \quad P_T^{\tau} > 20 \text{ GeV}, \quad |\eta^{\tau}| < 2.5. \tag{28}$$

   Notice we take the hadronic decays of the tau leptons. The tau tagging in Delphes3 is encoded with the origin of jets from hadronic decay modes of the tau lepton with an efficiency 0.6 and the misidentification rate from light-jet to tau-jet 0.01. The charge of tau-jet can be determined and reconstructed from the charged pions in the final state according to the algorithm inside Delphes3. The cross sections for both signal and backgrounds are shown in the second row of Table VI.

3. The forward jet pair is also required to be energetic with the following selection cuts

$$N(j) > 2, \qquad p_T^j > 30 \text{ GeV}, \qquad |\eta^j| < 5, \qquad m_{jj} > 500 \text{ GeV} . \tag{29}$$

   The cross sections after this step for both signal and backgrounds are shown in the third row of Table VI.

4. Since the major background comes from the $t\bar{t}$ associated processes, we apply b-jet veto to suppress background events:

$$N(b) = 0 \quad \text{with} \quad P_T^b > 20 \text{ GeV}, \quad |\eta^b| < 2.5. \tag{30}$$

   The cross sections after this step for both signal and background events are shown in the fourth row of Table VI.

5. The kinematical distributions of $M_{l^{\pm}\tau^+\tau^-}$ and $M_{\tau^+\tau^-}$ with $m_{H^{\pm}} = 205$ GeV and $m_{A^0} = 65$ GeV for the signal and backgrounds are shown in Fig. 9. Note that we have applied all the selection cuts except for $m_{H^{\pm}}$ and m_{A^0} cuts in these two kinematical

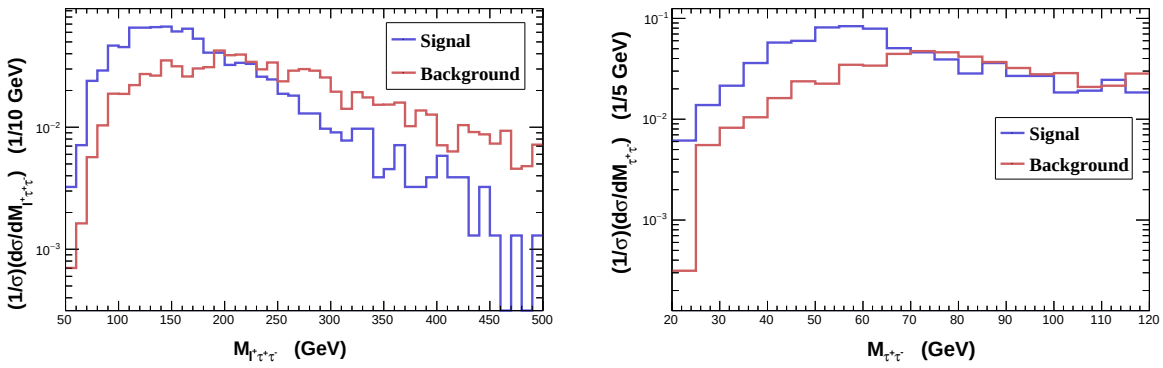

FIG. 9. Invariant mass distributions of $M_{l^\pm\tau^+\tau^-}$ (left panel) and $M_{\tau^+\tau^-}$ (right panel) for the signal with $m_{H^\pm} = 205$ GeV, $m_{A^0} = 65$ GeV, $\Delta m = 200$ GeV, $\tan\beta = 5$ and $\sin(\beta-\alpha) = 0.97$, and the total background at $\sqrt{s} = 14$ TeV. Preselection cuts in Eqs. (28), (29) and (30) are imposed.

distributions. The signal and background distributions of $M_{l^\pm\tau^+\tau^-}$ are similar to $M_{bbl^\pm}$ in Fig. 7. However, the peak shape at 65 GeV in $M_{\tau^+\tau^-}$ distribution for the signal from the resonance of A^0 is not so obvious compared with M_{bb} distribution in Fig. 7. The reason is that the τ-tagging is not as effective as b-tagging. On the other hand, since there are always neutrinos in τ lepton decays, the τ lepton cannot be fully reconstructed. This also explains why the shift of fat peak shape from 65 GeV to a slightly lower $M_{\tau^+\tau^-}$.

6. Finally, in order to further reduce the contributions from SM backgrounds, the following selection cuts are imposed on both signal and background events. For $m_{H^\pm}$ cuts at least two opposite-sign tau leptons and a lepton have to satisfy

$$M_{l^\pm\tau^+\tau^-} \leq M_{H^\pm} + 45 \text{ GeV}. \tag{31}$$

For the m_{A^0} cut at least a pair of opposite-sign tau leptons is required to around the mass of A^0:

$$m_{A^0} - 25 \text{ GeV} \leq M_{\tau^+\tau^-} \leq m_{A^0} + 35 \text{ GeV}. \tag{32}$$

The cross sections for both signal and background events after this sequence of event selection cuts are shown in the last two rows of Table VI.

TABLE VII. Cut flow table for the Type-X 2HDM signal $pp \to H^{\pm}H^{\pm}j_F j_F$ with $m_{H^{\pm}} = 205$ GeV, $m_{A^0} = 65$ GeV, $\Delta m = 200$ GeV, $\tan\beta = 5$ and $\sin(\beta-\alpha) = 0.97$, and various backgrounds at $\sqrt{s} = 27$ TeV.

Cross section (fb)	signal	$t\bar{t}Zjj$	$t\bar{t}W^{\pm}jj$	$W^{\pm}W^{\mp}Zjj$	$W^{\pm}ZZjj$
Preselection	9.93×10^{-2}	2.51	1.49	1.51×10^{-1}	8.62×10^{-3}
$N(\tau, l^{\pm}) \geq 3, 2,$ $P_T^{\tau,l^{\pm}} > 20$GeV,$\lvert\eta^{\tau,l}\rvert < 2.5$	4.27×10^{-3}	4.96×10^{-2}	6.14×10^{-3}	1.71×10^{-3}	4.04×10^{-4}
$N(j) \geq 2,$ $P_T^{j} > 30$GeV,$M_{jj} > 500$GeV	3.71×10^{-3}	3.69×10^{-2}	4.50×10^{-3}	1.08×10^{-3}	2.67×10^{-4}
b-jet veto	3.40×10^{-3}	9.23×10^{-3}	1.41×10^{-3}	9.23×10^{-4}	2.19×10^{-4}
$m_{H^{\pm}}$ Cut $M_{\tau^+\tau^-l^{\pm}} < 200$GeV	2.75×10^{-3}	4.04×10^{-3}	4.17×10^{-4}	3.94×10^{-4}	1.09×10^{-4}
m_{A^0} Cut $40 < M_{\tau^+\tau^-} < 70$GeV	2.35×10^{-3}	2.20×10^{-3}	1.96×10^{-4}	2.29×10^{-4}	6.63×10^{-5}

Again, even we can get a good signal-to-background ratio, the total number of events is still small. We further extend the signal-background analysis to the proposed 27 TeV pp collider (HE-LHC). Similar as before, we tighten both $m_{H^{\pm}}$ and m_{A^0} cuts relative to those in Eqs. (31) and (32). For $m_{H^{\pm}}$ cuts at least two tau leptons and a lepton have to satisfy

$$M_{\tau^+\tau^-l^{\pm}} \leq M_{H^{\pm}} - 5 \text{ GeV}. \tag{33}$$

For m_{A^0} cuts at least a pair of opposite-sign tau leptons is required to around the mass of A^0:[8]

$$m_{A^0} - 25 \text{ GeV} \leq M_{\tau^+\tau^-} \leq m_{A^0} + 5 \text{ GeV}. \tag{34}$$

Other preselection cuts in Eqs. (28), (29) and (30) are imposed, as before. We choose the same signal benchmark point to illustrate the cut flow under a sequence of selection cuts at $\sqrt{s} = 27$ TeV in Table VII.

Finally, we summarize the results for signal-background analysis of Type-X 2HDM at $\sqrt{s} = 27$ TeV with luminosity $\mathcal{L} = 15ab^{-1}$ in Fig. 10. The preselection cuts in Eqs. (28),

[8] Here we apply an asymmetric mass window cut for $M_{\tau^+\tau^-}$ based on the shift of peak shape in the right panel of Fig. 9 and in order to veto the pair of opposite-sign tau leptons from the Z-pole.

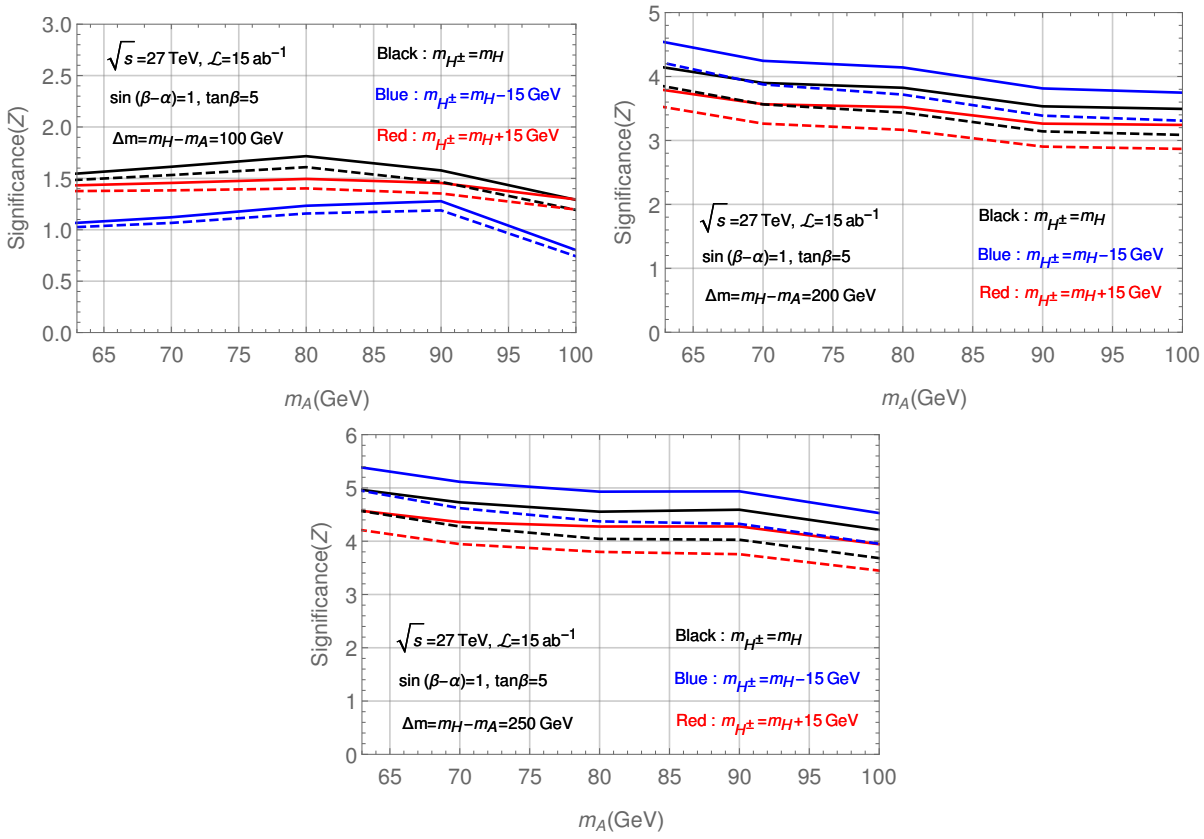

FIG. 10. The same as Fig. 8, but in Type-X 2HDM.

(29), (33) and (34) are imposed as before. We vary m_{A^0} from 63 to 100 GeV with fixed $\sin(\beta-\alpha)=1$ and $\tan\beta=5$ for $\Delta m=m_{H^0}-m_{A^0}=100$ GeV (upper-left panel), 200 GeV (upper-right panel), and 250 GeV (lower panel) in Fig. 10 as the illustrative examples. The black lines are $m_{H^\pm}=m_{H^0}$, the blue lines are $m_{H^\pm}=m_{H^0}-15$ GeV, and the red lines are $m_{H^\pm}=m_{H^0}+15$ GeV. The maximum significance can reach to about $Z=1.7$ at $m_{A^0}=80$ GeV for $\Delta m=100$ GeV. Notice that the mass spectrum with $\Delta m=100$ GeV and $m_{H^\pm}=m_{H^0}-15$ GeV in Type-X 2HDM will produce sizable $B(H^\pm\to\tau\nu_\tau)$ and suppress $B(H^\pm\to W^\pm A^0)$. That makes reduction of the significance for the blue line in the upper-left panel in Fig. 10. On the other hand, the significance can reach to more than $Z=3$ for m_{A^0} from 63 GeV to 100 GeV with $\Delta m=200$ GeV, and its maximum is about $Z=4.5$ at $m_{A^0}=63$ GeV. Moreover, the significance can grow to more than $Z=4$ for m_{A^0} from 63 GeV to 100 GeV with $\Delta m=250$ GeV, and its maximum can further reach to $Z=5.4$ at $m_{A^0}=63$ GeV. Again, the 5% systematic errors of the SM background events in Eq. (23) are shown as dashed lines in Fig. 10 for comparisons.

V. CONCLUSIONS

Extending the minimal Higgs sector is one of the approaches to address some weakness of the SM. Such extensions can give rise to rich phenomenology. The 2HDM is one of the most popular extended models in literature. Exploring the whole mass spectrum in 2HDM is undoubtedly an important mission to help us understand the mystery of electroweak symmetry breaking. There are only a few examples that can cover the effects of all new scalar masses in a single process. We have studied a novel process – production of same-sign charged Higgs production shown in Eq. (1), which was first proposed in Ref. [26]. It allows one to probe the whole mass spectrum in the 2HDM for some specific mass relations.

We have investigated same-sign charged Higgs-boson production via vector-boson-fusion at the HL-LHC and HE-LHC (27 TeV) in Type I and X 2HDM's. The dependence of the production cross section on the mass difference $\Delta m \equiv m_{H^0} - m_{A^0}$ between the heavier scalar boson H^0 and the pseudoscalar boson A^0 is studied. The scattering amplitude of the key subprocess $W^+W^+ \to H^+H^+$ is proportional to Δm as shown in Eq. (9), such that the production cross section nearly vanishes in the limit $\Delta m \to 0$. As we mentioned before, even if the mass splitting Δm can be determined by separately measuring m_{H^0} and m_{A^0} from other production channels of H^0 and A^0, the measurement of same-sign charged Higgs-boson production cross section can be used to understand the mass spectrum of the heavier scalar and pseudoscalar bosons in the 2HDMs.

Given the constraints from electroweak precision, B physics, and direct searches at colliders, we have explored the allowed parameter space in $m_{H^\pm}$, $\tan\beta$, Δm. Then we investigated the sensitivity to the allowed parameter space at the HL-LHC and HE-LHC, especially we have made use of the bosonic channel $W^\pm A^0$ of the charged Higgs boson, which is complementary to the study in Ref. [26].

In type I 2HDM, we used the decay channel $H^\pm H^\pm \to (W^\pm A^0)(W^\pm A^0) \to (l^\pm \nu b\bar{b})\,(l^\pm \nu b\bar{b})$ together with a pair of forward jets to perform the signal-background analysis. At the end, we found about 4 signal events versus 5 background events at HL-LHC with luminosity of 3000 fb^{-1} for a typical benchmark point. At the HE-LHC, significance level of $2.6 - 5.8$ can be achieved for $\Delta m = 200 - 250$ GeV.

On the other hand, in type X 2HDM we used the decay channel $H^\pm H^\pm \to (W^\pm A^0)(W^\pm A^0) \to (l^\pm \nu \tau^+ \tau^-)\,(l^\pm \nu \tau^+ \tau^-)$ together with a pair of forward jets to perform the signal-background

analysis. At the HL-LHC, we can achieve the signal-to-background ratio equal to 1, and the number of signal events is about 2 for a luminosity of 3000 fb^{-1}. Nevertheless, at the HE-LHC the significance can rise to the level of $3.2 - 5.4$ for $\Delta m = 200 - 250$ GeV.

The main purpose of this study focuses on the search for a possible large mass splitting between the neutral scalar and pseudoscalar through same-sign charged-Higgs-boson production in 2HDMs via the vector-boson fusion. It is easy to see that this is not the discovery mode of the charged Higgs because the event rate is much lower than other direct processes, e.g., $gb \to tH^-$ or $gg \to t\bar{b}H^-$. " According to Ref. [12, 40] for the search of $gb \to tH^-$ or $gg \to t\bar{b}H^-$ with $H^- \to \tau^-\overline{\nu}_\tau$, the constrained region is $\tan\beta \lesssim 2\,(4)$ in type-I (type-X) 2HDM for the mass range $160 \leq M_{H^\pm} \leq 180$ GeV and there is no constraint for $M_{H^\pm} > 180$ GeV.

Notice that the process in Eq. (1) can be used to distinguish between the charged Higgs boson from a doublet and a triplet. Here, we take the Y=2 triplet model (type II seesaw) as an example. In this model, the triplet VEV is highly constrained from electroweak precision measurement to be less than a few GeV [58–60]. On the other hand, both $m_{H^\pm}$ and m_{A^0} in this model are close to degenerate, therefore $H^\pm \to W^\pm A^0$ is very suppressed. The observation of such decay would exclude type II seesaw model.

For the VEV of triplet around 1 GeV and $m_{H^\pm} < 400$ GeV, the three dominant $H^\pm$ decay modes, $H^\pm \to \{W^\pm h, W^\pm Z, tb\}$, are competitive [58]. If one can reconstruct the Z/h invariant mass in the final state, it would be viewed as a clear signal beyond 2HDMs in the alignment limit. In the process in Eq. (1), besides the t-channel Z boson exchange and s-channel doubly charged Higgs contributions for the same-sign charged Higgs pair production would also show the differences between the triplet model and 2HDMs.

However, in the case of tiny triplet VEV and high triplet mass scale, $H^\pm \to \{W^\pm h, W^\pm Z\}$ and also $H^{\pm\pm}W^\mp W^\mp$ couplings would be very suppressed. Therefore, the dominant decay mode of $H^\pm$ turns out to be $H^\pm \to l\nu_l$ and the doubly charged Higgs contribution in same-sign charged Higgs pair production would be small. Besides, because of the mass degeneracy between A^0 and $H^\pm$ in the Y=2 triplet model, we would not have $H^\pm \to W^\pm A^0$ decay mode. In the end, for the case of tiny triplet VEV, even the triplet model can mimic the same-sign charged higgs pair production with $H^\pm \to \tau\nu_\tau$ in 2HDMs as shown in Ref. [26]. The $H^\pm \to W^\pm A^0$ decay mode in this work can help us to distinguish 2HDMs from the triplet model.

One can also advocate $H^\pm \to W^\pm A^0$ decay channel to distinguish the 2HDM from the Minimal Supersymmetric Standard Model (MSSM) which is a 2HDM of type II. However, because of the MSSM sum rules [61], we have $m^2_{H^\pm} = m^2_{A^0} + m^2_W$ which makes the decay channel $H^\pm \to W^\pm A^0$ not open very often and turn out to be rather small. In fact, in the MSSM, $Br(H^\pm \to W^\pm A^0)$ is very suppressed (less than 10^{-2}) while $Br(H^\pm \to W^\pm h^0)$ is of the order of a few percent [62]. Therefore, the dominant decay of $H^\pm$ are $\tau\nu$ for low charged Higgs mass and tb for $m_{H^\pm} > m_t + m_b$. In this case also, the MSSM will mimic the same-sign charged higgs pair production with $H^\pm \to \{\tau\nu_\tau, tb\}$ in 2HDMs as shown in Ref. [26].

In summary, the process in Eq. (1) can be an additional check of the mass relation between same-sign charged Higgs-boson production and Δm, especially, if the 2HDM mass spectrum has the following relations:

- one light (pseudo)scalar, say A^0,
- a large mass splitting between two neutral scalars, $\Delta m = (m_{H^0} - m_{A^0})$, and
- the charged Higgs mass is above the $W^\pm A^0$ threshold,

then this scenario in the 2HDMs can be either pinned down or ruled out in the future.

ACKNOWLEDGMENT

The work of K.C. was supported by the National Science Council of Taiwan under Grants Nos. MOST-105-2112-M-007-028-MY3 and MOST-107-2112-M-007-029-MY3. AA is supported in part by the Moroccan Ministry of Higher Education and Scientific Research under Contract N'PPR/2015/6 . AA would like to thank NCTS for hospitality, where this work has been done.

[1] T. D. Lee, Phys. Rev. D **8**, 1226 (1973). doi:10.1103/PhysRevD.8.1226

[2] G. C. Branco, P. M. Ferreira, L. Lavoura, M. N. Rebelo, M. Sher and J. P. Silva, Phys. Rept. **516**, 1 (2012) doi:10.1016/j.physrep.2012.02.002 [arXiv:1106.0034 [hep-ph]].

[3] S. L. Glashow and S. Weinberg, Phys. Rev. D **15**, 1958 (1977). doi:10.1103/PhysRevD.15.1958

[4] V. D. Barger, R. J. N. Phillips and D. P. Roy, Phys. Lett. B **324**, 236 (1994) doi:10.1016/0370-2693(94)90413-8 [hep-ph/9311372].

[5] A. G. Akeroyd *et al.*, Eur. Phys. J. C **77**, no. 5, 276 (2017) doi:10.1140/epjc/s10052-017-4829-2 [arXiv:1607.01320 [hep-ph]].

[6] G. Abbiendi *et al.* [ALEPH and DELPHI and L3 and OPAL and LEP Collaborations], Eur. Phys. J. C **73**, 2463 (2013) doi:10.1140/epjc/s10052-013-2463-1 [arXiv:1301.6065 [hep-ex]].

[7] V. M. Abazov *et al.* [D0 Collaboration], Phys. Rev. D **80**, 051107 (2009) doi:10.1103/PhysRevD.80.051107 [arXiv:0906.5326 [hep-ex]].

[8] JHEP **1503**, 088 (2015) [arXiv:1412.6663 [hep-ex]].

[9] M. Aaboud *et al.* [ATLAS Collaboration], JHEP **1809** (2018) 139 doi:10.1007/JHEP09(2018)139 [arXiv:1807.07915 [hep-ex]].

[10] M. Aaboud *et al.* [ATLAS Collaboration], Phys. Lett. B **759**, 555 (2016) [arXiv:1603.09203 [hep-ex]].

[11] V. Khachatryan *et al.* [CMS Collaboration], JHEP **1511**, 018 (2015) [arXiv:1508.07774 [hep-ex]].

[12] A. M. Sirunyan *et al.* [CMS Collaboration], arXiv:1903.04560 [hep-ex].

[13] CMS Collaboration [CMS Collaboration], CMS-PAS-HIG-16-031.

[14] G. Aad *et al.* [ATLAS Collaboration], Eur. Phys. J. C **73**, no. 6, 2465 (2013) doi:10.1140/epjc/s10052-013-2465-z [arXiv:1302.3694 [hep-ex]].

[15] The ATLAS collaboration [ATLAS Collaboration], ATLAS-CONF-2016-089.

[16] M. Aaboud *et al.* [ATLAS Collaboration], JHEP **1811**, 085 (2018) doi:10.1007/JHEP11(2018)085 [arXiv:1808.03599 [hep-ex]].

[17] CMS Collaboration [CMS Collaboration], CMS-PAS-HIG-18-004.

[18] CMS Collaboration [CMS Collaboration], CMS-PAS-HIG-18-015.

[19] A. Arhrib, R. Benbrik and S. Moretti, Eur. Phys. J. C **77**, no. 9, 621 (2017) doi:10.1140/epjc/s10052-017-5197-7 [arXiv:1607.02402 [hep-ph]].

[20] F. Kling, A. Pyarelal and S. Su, JHEP **1511**, 051 (2015) doi:10.1007/JHEP11(2015)051 [arXiv:1504.06624 [hep-ph]].

[21] B. Coleppa, F. Kling and S. Su, JHEP **1412**, 148 (2014) doi:10.1007/JHEP12(2014)148 [arXiv:1408.4119 [hep-ph]].

[22] R. Dermisek, E. Lunghi and A. Raval, JHEP **1304**, 063 (2013) doi:10.1007/JHEP04(2013)063 [arXiv:1212.5021 [hep-ph]].

[23] A. G. Akeroyd, A. Arhrib and Q. S. Yan, Eur. Phys. J. C **55**, 653 (2008) doi:10.1140/epjc/s10052-008-0617-3 [arXiv:0712.3933 [hep-ph]].

[24] J. Abdallah *et al.* [DELPHI Collaboration], Eur. Phys. J. C **34**, 399 (2004) doi:10.1140/epjc/s2004-01732-6 [hep-ex/0404012].

[25] A. M. Sirunyan *et al.* [CMS Collaboration], Phys. Rev. Lett. **123**, no. 13, 131802 (2019) doi:10.1103/PhysRevLett.123.131802 [arXiv:1905.07453 [hep-ex]].

[26] M. Aiko, S. Kanemura and K. Mawatari, Phys. Lett. B **797**, 134854 (2019) doi:10.1016/j.physletb.2019.134854 [arXiv:1906.09101 [hep-ph]].

[27] M. Aoki, S. Kanemura, K. Tsumura and K. Yagyu, Phys. Rev. D **80**, 015017 (2009) doi:10.1103/PhysRevD.80.015017 [arXiv:0902.4665 [hep-ph]].

[28] V. D. Barger, J. L. Hewett and R. J. N. Phillips, Phys. Rev. D **41**, 3421 (1990). doi:10.1103/PhysRevD.41.3421

[29] B. W. Lee, C. Quigg and H. B. Thacker, Phys. Rev. D **16**, 1519 (1977). doi:10.1103/PhysRevD.16.1519

[30] S. Kanemura, T. Kubota and E. Takasugi, Phys. Lett. B **313**, 155 (1993) doi:10.1016/0370-2693(93)91205-2 [hep-ph/9303263].

[31] S. Kanemura and K. Yagyu, Phys. Lett. B **751**, 289 (2015) doi:10.1016/j.physletb.2015.10.047 [arXiv:1509.06060 [hep-ph]].

[32] M. Tanabashi *et al.* [Particle Data Group], Phys. Rev. D **98**, no. 3, 030001 (2018). doi:10.1103/PhysRevD.98.030001

[33] H. E. Haber and A. Pomarol, Phys. Lett. B **302**, 435 (1993) doi:10.1016/0370-2693(93)90423-F [hep-ph/9207267].

[34] M. Misiak and M. Steinhauser, Eur. Phys. J. C **77**, no. 3, 201 (2017) doi:10.1140/epjc/s10052-017-4776-y [arXiv:1702.04571 [hep-ph]].

[35] M. Misiak *et al.*, Phys. Rev. Lett. **114**, no. 22, 221801 (2015) doi:10.1103/PhysRevLett.114.221801 [arXiv:1503.01789 [hep-ph]].

[36] T. Enomoto and R. Watanabe, JHEP **1605**, 002 (2016) doi:10.1007/JHEP05(2016)002 [arXiv:1511.05066 [hep-ph]].

[37] J. Haller, A. Hoecker, R. Kogler, K. Mönig, T. Peiffer and J. Stelzer, Eur. Phys. J. C **78**, no. 8, 675 (2018) doi:10.1140/epjc/s10052-018-6131-3 [arXiv:1803.01853 [hep-ph]].

[38] D. Eriksson, J. Rathsman and O. Stal, Comput. Phys. Commun. **181**, 189 (2010) doi:10.1016/j.cpc.2009.09.011 [arXiv:0902.0851 [hep-ph]].

[39] G. Aad *et al.* [ATLAS Collaboration], JHEP **1603**, 127 (2016) doi:10.1007/JHEP03(2016)127 [arXiv:1512.03704 [hep-ex]].

[40] P. Sanyal, Eur. Phys. J. C **79**, no. 11, 913 (2019) doi:10.1140/epjc/s10052-019-7431-y [arXiv:1906.02520 [hep-ph]].

[41] A. M. Sirunyan *et al.* [CMS Collaboration], JHEP **1811**, 161 (2018) doi:10.1007/JHEP11(2018)161 [arXiv:1808.01890 [hep-ex]].

[42] A. M. Sirunyan *et al.* [CMS Collaboration], JHEP **1905**, 210 (2019) doi:10.1007/JHEP05(2019)210 [arXiv:1903.10228 [hep-ex]].

[43] A. M. Sirunyan *et al.* [CMS Collaboration], Phys. Lett. B **793**, 320 (2019) doi:10.1016/j.physletb.2019.03.064 [arXiv:1811.08459 [hep-ex]].

[44] The ATLAS collaboration [ATLAS Collaboration], ATLAS-CONF-2018-025.

[45] M. Aaboud *et al.* [ATLAS Collaboration], Phys. Lett. B **790**, 1 (2019) doi:10.1016/j.physletb.2018.10.073 [arXiv:1807.00539 [hep-ex]].

[46] A. M. Sirunyan *et al.* [CMS Collaboration], Phys. Lett. B **785**, 462 (2018) doi:10.1016/j.physletb.2018.08.057 [arXiv:1805.10191 [hep-ex]].

[47] M. Aaboud *et al.* [ATLAS Collaboration], JHEP **1810**, 031 (2018) doi:10.1007/JHEP10(2018)031 [arXiv:1806.07355 [hep-ex]].

[48] A. M. Sirunyan *et al.* [CMS Collaboration], Phys. Lett. B **795**, 398 (2019) doi:10.1016/j.physletb.2019.06.021 [arXiv:1812.06359 [hep-ex]].

[49] A. M. Sirunyan *et al.* [CMS Collaboration], JHEP **1811**, 018 (2018) doi:10.1007/JHEP11(2018)018 [arXiv:1805.04865 [hep-ex]].

[50] M. Aaboud *et al.* [ATLAS Collaboration], Phys. Lett. B **783**, 392 (2018) doi:10.1016/j.physletb.2018.07.006 [arXiv:1804.01126 [hep-ex]].

[51] P. Bechtle, O. Brein, S. Heinemeyer, O. Stål, T. Stefaniak, G. Weiglein and K. E. Williams, Eur. Phys. J. C **74**, no. 3, 2693 (2014) doi:10.1140/epjc/s10052-013-2693-2 [arXiv:1311.0055 [hep-ph]].

[52] P. Bechtle, S. Heinemeyer, O. Stål, T. Stefaniak and G. Weiglein, Eur. Phys. J. C **74**, no. 2, 2711 (2014) doi:10.1140/epjc/s10052-013-2711-4 [arXiv:1305.1933 [hep-ph]].

[53] C. Degrande, Comput. Phys. Commun. **197**, 239 (2015) doi:10.1016/j.cpc.2015.08.015 [arXiv:1406.3030 [hep-ph]].

[54] J. Alwall *et al.*, JHEP **1407**, 079 (2014) doi:10.1007/JHEP07(2014)079 [arXiv:1405.0301 [hep-ph]].

[55] T. Sjostrand, S. Mrenna and P. Z. Skands, Comput. Phys. Commun. **178**, 852 (2008) doi:10.1016/j.cpc.2008.01.036 [arXiv:0710.3820 [hep-ph]].

[56] J. de Favereau *et al.* [DELPHES 3 Collaboration], JHEP **1402**, 057 (2014) [arXiv:1307.6346 [hep-ex]].

[57] E. Conte, B. Fuks and G. Serret, Comput. Phys. Commun. 184 (2013) 222, [arXiv:1206.1599 [hep-ph]] ;E. Conte, B. Dumont, B. Fuks and C. Wymant, Eur. Phys. J. C 74 (2014) 10, 3103, [arXiv:1405.3982 [hep-ph]] ;B. Dumont, B. Fuks, S. Kraml et al., Eur. Phys. J. C 75 (2015) 2, 56, [arXiv:1407.3278 [hep-ph]].

[58] P. Fileviez Perez, T. Han, G. y. Huang, T. Li and K. Wang, Phys. Rev. D **78**, 015018 (2008) doi:10.1103/PhysRevD.78.015018 [arXiv:0805.3536 [hep-ph]].

[59] A. Melfo, M. Nemevsek, F. Nesti, G. Senjanovic and Y. Zhang, Phys. Rev. D **85**, 055018 (2012) doi:10.1103/PhysRevD.85.055018 [arXiv:1108.4416 [hep-ph]].

[60] A. Arhrib, R. Benbrik, M. Chabab, G. Moultaka, M. C. Peyranere, L. Rahili and J. Ramadan, Phys. Rev. D **84**, 095005 (2011) doi:10.1103/PhysRevD.84.095005 [arXiv:1105.1925 [hep-ph]].

[61] J. F. Gunion, H. E. Haber and J. Wudka, Phys. Rev. D **43**, 904 (1991). doi:10.1103/PhysRevD.43.904

[62] A. Djouadi, Phys. Rept. **459**, 1 (2008) doi:10.1016/j.physrep.2007.10.005 [hep-ph/0503173].